

EXPERIMENTAL DETERMINATION OF NONLINEAR NORMAL MODES OF A  
CIRCULAR PERFORATED PLATE

By

Ryan B. Harris

A thesis submitted in partial fulfillment of  
the requirements for the degree of

Master of Science  
(Mechanical Engineering)

at the

UNIVERSITY OF WISCONSIN-MADISON

December 2014



## Table of Contents

Abstract.....	iii
Nomenclature.....	v
Acknowledgements.....	vi
1. Introduction .....	1
1.1 Nonlinear Normal Modes (NNMs) .....	3
2. The Cummins Perforated Plate.....	6
2.1 Test Specimen .....	7
3. Linear Analysis of Circular Perforated Plates .....	9
3.1 Finite Element Model.....	17
3.2 Roving Hammer Tests.....	20
3.3 Comparison of the Linear Analysis of the Circular Perforated Plate.....	21
4. Experimental Setup for Small Shaker .....	27
4.1 First Mode of Vibration on Small Shaker .....	35
4.2 Fourth, Fifth, and Sixth Modes of Vibration on Small Shaker .....	38
4.3 Comparison of Numerical Models to Small Shaker Tests .....	46
5. Experimental Setup for Large Shaker Tests .....	54
5.1 First mode of Vibration on Large Shaker.....	57
5.2 Second and Third Modes of Vibration on Large Shaker .....	65

5.3	Fifth and Sixth Modes of Vibration on Large Shaker .....	69
5.4	Comparison of Small Shaker to Large Shaker NNMs .....	73
6.	Conclusion .....	74
7.	Future Work .....	76
8.	References .....	78

**Abstract**

In the engineering design process, linear vibration analysis is a common practice and the widely used theory of linear normal modes (LNMs) is used to analyze and gather the structures invariants. However, linearity is an ideal situation in real life and overlooking nonlinearity can often lead to premature failure of the design. It is for this reason that an experimental method needs to be developed that can properly treat nonlinear vibrations in structures, using the theory of nonlinear normal modes (NNMs). NNMs are an extension of the commonly used LNMs; however, the NNMs are used in the nonlinear response range by using a predetermined input energy and evaluating the unforced vibration response. Recently, there have been great advances in experimental methods that attempt to estimate NNMs by using periodic excitations to isolate single NNMs. These experimentally obtained NNMs can then be used to verify the validity of finite element models of the system. This thesis explores a new approach to experimentally obtain NNMs and then uses a finite element model for comparison and updating.

The structure under which the new experimental method will be tested on in this thesis is a circular perforated plate, and to begin with, a linear modal analysis was performed to verify that the natural frequencies and mode shapes in the linear vibrating region were accurate. This was performed by comparing the theoretical natural frequencies and mode shapes to the finite element model and an impact roving hammer test with very low force levels. It was found that within the linearly vibrating region the finite element model was fairly accurate for most modes of vibration.

Following the linear evaluation of the plate, shaker tests on a relatively small shaker were performed on the plate on the first, fourth, fifth and sixth modes of vibration to test the robustness of the methodology. The NNM's were extracted from the frequency response functions (FRFs) of the tests and the validity of the NNMs was confirmed using the phase lag quadrature criterion. The results of the tests showed that the method presented in this thesis was able to obtain the NNMs of the structure with good accuracy for most of the modes. However, other dynamics became apparent in the analysis of the results when comparisons with the finite element analysis were made. Therefore, further investigation into the test specimens was performed and an updated finite element model was created.

In order to verify the newly updated model, the specimen was tested again on a larger shaker that could induce a much higher response. The same methodology was used on the large shaker to obtain the NNMs. The results of which were mixed, because the phase lag quadrature criterion was not met as easily for most of the modes. Therefore, the NNMs that were extracted on the large shaker are not as valid as those extracted on the smaller shaker. However, they still produced an adequate estimate of the NNM. The majority of the cases presented in this thesis proved that the new experimental method to extract NNMs from nonlinear systems was a success, as many of the experiments were able to capture the NNMs of the system with good accuracy and displayed the nonlinear characteristics of the system.

## Nomenclature

Arranged in alphabetical order

$a$ - radius of plate	$M_\theta$ - tangential moment
$A_m$ - coefficient constant	$M_{\theta r}$ - twisting moment
$a_{ccel}$ - acceleration	$\nu$ - Poisson's ratio
$B_m$ - coefficient constant	$\omega$ - transverse displacement
$C_m^{(1)}$ - constant based on boundary conditions of plate	$\omega_{mn}$ - natural frequency of mode of vibration with $m$ number of nodal diameters and $n$ number of nodal circles
$C_m^{(2)}$ - constant based on boundary conditions of plate	$Q_r$ - transverse shear force in radial direction
$C_m^{(3)}$ - constant based on boundary conditions of plate	$Q_\theta$ - transverse shear force in tangential direction
$C_m^{(4)}$ - constant based on boundary conditions of plate	$r$ - a radius
$D$ - flexural rigidity	$\rho$ - density
$\nabla$ - biharmonic operator	$T$ - time variable of transverse displacement
$E$ - Young's modulus	$t$ - time
$f$ - transverse force applied to the plate element	$\theta$ - an angle
$F_a$ - forcing amplitude	$W$ - spatial variable of transverse displacement
$g$ - acceleration due to gravity	$Y_m$ - Bessel function of the second kind of order $m$
$h$ - height of the plate	
$I_m$ - modified Bessel function of the first kind of order $m$	
$J_m$ - Bessel function of the first kind of order $m$	
$K_m$ - modified Bessel function of the second kind of order $m$	
$\lambda_{mn}$ - eigenvalues of mode of vibration with $m$ number of nodal diameters and $n$ number of nodal circles	
$M$ - mass	
$M_r$ - radial moment	
$M_{r\theta}$ - twisting moment	

## **Acknowledgements**

I would sincerely like to thank my advising Professor, Matthew S. Allen for allowing me the opportunity to work with him and his group on this research project. I would also like to thank him for assisting me in my endeavors and lending his expertise on this thesis. I would especially like to thank him when it comes to his patience with me trying to juggle all of my activities while at The University of Wisconsin-Madison.

I would also like to thank David Ehrhardt for all of his help with teaching me about vibrational testing and data processing. I wouldn't have been able to complete this thesis without his assistance and knowledge.

I am grateful for Rob Kuether's work on the finite element models that was used in this thesis in order to make comparisons. This thesis would have been very different without his work and I would like to thank him for that.

I also acknowledge the general support of the Air Force Office of Scientific Research under grant number FA9550-11-1-0035, administered by the Dr. David Stargel of the Multi-Scale Structural Mechanics and Prognosis Program.

Finally, I would like to acknowledge and thank Peter Penegor and David Nickel from Cummins Emission Solutions for providing the perforated plate test specimens.



## 1. Introduction

In the world of engineering design, the common use of a purely linear vibrating system usually results in a sub-optimum design, as nonlinearities are a common occurrence in real-life. Linear systems are described as systems where all system invariants, such as frequency-response functions, damping ratios, mode shapes, and resonant frequencies; are governed by their respective linear differential equations. However, simply because a system may act in a linear manner within certain parameters does not substantiate the fact that the system is truly linear. As a result of only looking at systems in their linear range, nonlinearities are often overlooked. This can easily be done because nonlinearities may be caused by something as simple as geometry or friction. On the other hand, it can be a result of something as complex as the interactions of two different interfacing materials. Furthermore, nonlinearities are often dependent on the frequency at which the system is vibrating and the energy applied to the system. The more energy that is applied to the system the greater the chance of leaving a linearly acting region for a nonlinear one. Therefore, it is imperative that the engineering design process focus on methods to improve nonlinear design.

In classical vibration analysis the theory of linear systems has been paramount and within this theory lies the concept of linear normal modes (LNMs). One important property of LNMs is their ability to decouple the equations of motion, or create independent linear vibrating systems regulated by their eigensolutions. As a result of decoupling the equations of motion, two principles arise that are quite useful in linear vibration analysis. The first being that of invariance, where when motion is initiated on

an individual LNM all other LMNs are quiescent for all time. The other principle is that of modal superposition, and it is defined as the ability to combine all individual LNM motion for both free and forced oscillations. However, as previously stated a linear analysis of a system will only produce a sub-optimum design and therefore an analysis technique for nonlinear systems is necessary. One such analysis technique is that of nonlinear normal modes (NNMs). Nonlinear normal modes are a powerful tool for structural design that allows an engineer to easily comprehend a structure's free and forced response for a variety of nonlinear dynamic behavior and relate them to the LNM that are so widely used.

This thesis purposes a variation on established testing techniques for experimentally extracting the backbone curves to estimate NNMs, using an extension of force appropriation common in linear experimental modal analysis (EMA), in conjunction with the phase lag quadrature criterion. The force appropriation technique is used to isolate single LNM by exciting the structure under examination at key locations. This is accomplished by modifying the frequency and amplitude distribution of the excitation and allows for the modal parameters to be extracted from the isolated mode. The phase lag quadrature criterion states that when a phase shift of 90 degrees occurs between the excitation force and the acceleration of the response then resonance has been achieved.

The test specimen which the method will be tested on is a circular perforated plate provided by Cummins. The specimen was excited with modal shakers using a stepped-sine harmonic excitation at various forcing amplitudes to isolate single NNMs. The

NNMs are then estimated using the backbones of the nonlinear frequency responses. Multiple modes were tested to verify the robustness of the method. A finite element model was also generated to estimate the NNMs which are then compared to the experimental results and updated to attempt to properly capture the nonlinearity.

The results of the work done in this thesis are conveyed as follows. First, a linear analysis of the perforated plate was performed. Theoretically, numerically, and experimentally obtained natural frequencies and mode shapes were compared to verify the finite element model in the linear vibration region. This was followed by stepped-sine excitation of the circular perforated plate on a small modal shaker. The NNMs were then extracted from the nonlinear frequency responses and compared to the NNMs generated by the finite element model. Upon comparison it was seen that the physics of the plate were not properly modeled and an updated finite element model was developed. It was also seen in the model that the type of nonlinearity changed at higher forcing amplitudes and as a result, the circular plate was tested on a larger modal shaker to observe if in fact, the type of nonlinearity actually changed and if it could be captured by the NNM. Finally, conclusions of the method and future work on how to improve the experimental method are presented.

### **1.1 Nonlinear Normal Modes (NNMs)**

Nonlinear normal modes first began to be studied in the 1960's by R.M. Rosenberg [1, 2, 3], who defined a NNM as a *vibration in unison* of the system. In order for this definition to hold true then all the structures material points would simultaneously reach their maximum displacements and simultaneously pass through the reference zero.

However, this definition does not apply for most non-conservative systems or for all nonlinear phenomena, such as internal resonances. The existence of these issues requires that the definition of a NNM be redefined, such that it may envelope all nonlinear phenomena that may be encountered in engineering design. Kerschen et al [4] was able to do just this by extending Rosenbergs' definition to a not necessarily synchronous periodic motion of the conservative system. This definition is substantiated by the fact that motion with the existence of internal resonances; while not synchronous in nature, is still periodic. This is coupled with the research shown in [5,6] that displays that the damped dynamics of a system may be represented by the topology and bifurcations of the NNMs of the underlying damped system. The combination of these studies allows for Kerschens' extended definition to be viable.

Although powerful, NNMs do not follow two of the most important properties of LNs; the first being modal superposition and the second orthogonality. At first this may appear to discredit the applicable use of NNMs, but there are many useful properties of NNMs that make them effective in defining the invariants of nonlinear behavior. One of the unique properties of NNMs is the fact that they are frequency-energy dependent. This means that the resonant frequencies of a NNM are governed by the total energy that is applied to the system. It is this property that hinders the separation of variables in the systems governing equations of motion. However, this frequency-energy dependence can be represented in a frequency energy plot to display many of the characteristics exhibited by the nonlinear system. Another distinctive feature of NNMs is that their number can possibly surpass the number of degrees of freedom in a system. This is a direct result of internal resonances or even bifurcations. Bifurcations in a system can sometimes lead to

instability of a system which does not occur in LNMs. A great benefit of using NNMs is that they often display modal interactions such as internal resonances, which would be easily missed if only linear experimental techniques that are limited to small-amplitude motions are considered. There is no correlation between internally resonant NNMs and linear systems, making them unique to nonlinear analysis. Other important properties of NNMs are that the forced resonances in nonlinear systems occur around the location of NNMs. Therefore, the structure of the resonances can easily be characterized. Also, any system's damped dynamics have been shown to adhere to the NNMs of the underlying damped system. These properties make NNMs an important resource within nonlinear analysis and as a result they are receiving more attention as of late to better improve engineering design.

Since their inception, techniques used to numerically compute NNMs have been explored and recent advances in computing methods have greatly improved these techniques. For example, within the past few years Peeters et al.[7] presented a technique using numerical integration and continuation for a structure with hundreds of degrees of freedom as long as the nonlinearities are localized on the structure. This method was then used as the basis for Allen, Kuether & Deaner [8,9] to develop a means to model structures with many degrees of freedom and with geometric nonlinearities. They found that using Peeters et al's approach that structures with geometric nonlinearities may be modeled accurately within commercially available finite element software. Upon completion, Allen, Kuether & Brake [10] used the theory of NNMs to show that when the NNMs of a reduced order model (ROM) of a structure are correct, that the response of

the ROM will match the response of the full model for many initial conditions and types of forcing.

Experimental procedures to obtain NNMs have also been explored, although not as extensively as numerical computation methods. Peeters et al [20] recently developed a technique based on stepped-sine testing where a nonlinear extension of force appropriation is used to isolate a single NNM. Once the NNM had been isolated the excitation was removed and the system was allowed to decay; presumably along the NNM. Using the time-frequency analysis, a frequency energy plot was constructed that displayed the NNM and its characteristics. The authors also used the same technique on a beam with a local nonlinearity added at one end which produced fairly good results [11]. Similar to this thesis, Grappasonni et al [12] used a stepped-sine testing approach on a specimen with a geometric nonlinearity that was created by vastly changing the thickness of one end of a beam and clamping it in place. The NNMs were then used to verify the subspace estimation of the nonlinear parameters of the system.

## **2. The Cummins Perforated Plate**

This thesis was a product of a former investigation into the fatigue life of a diesel aftertreatment circular perforated exhaust plate for Cummins Emission Solutions. The exhaust plate was experiencing early cyclical loading failure and the reason was unknown. The University of Wisconsin-Madison further investigated the cause of the catastrophic failure. Initially the scope of the work done was focused on the stress concentrations on the plate due to the perforated holes. However, upon testing the specimen on a large shaker it became apparent that the system was behaving nonlinearly.

The scope of the project shifted to finding the origin of the nonlinearity in the system. It was thought to be beneficial to find a method to experimentally determine the NNMs of the circular plate to define the characteristics of the nonlinearity so that in turn an accurate finite element model may be generated.

## 2.1 Test Specimen

As previously mentioned, the specimen under investigation is a circular perforated plate with rolled ends which can be seen in Figure 1.

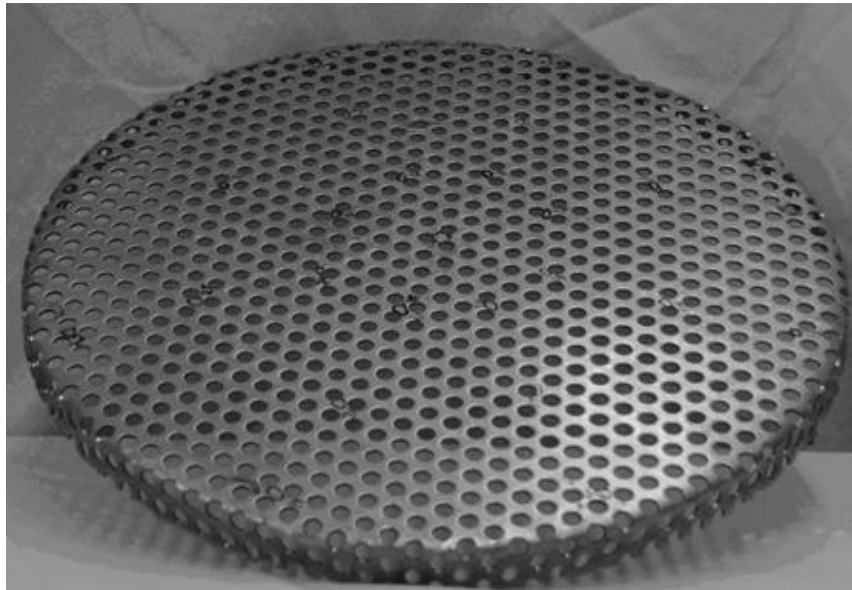


**Figure 1: Perforated plate**

The perforations in the plate were created using a mechanical punch in the flat 16 gauge (1.52 mm thick) 409 stainless steel plate. The perforations create a pattern of equilateral triangles with 10.16 mm long edges. The next step in creating the exhaust plate was to form it around a 317.5 mm diameter mold. The surplus steel was then cut away leaving a lip of 317.5 mm. Upon completion, the plate was welded to a 317.5 diameter, 14 gauge

(1.9 mm) thick, and 89 mm high cold rolled 409 stainless steel cylinder. The completed assembly can be seen in Figure 2. In order to conduct modal testing on the specimen it was necessary to attach it to a fixture that would allow for use on both a small modal shaker and a large modal shaker. In addition the boundary conditions of the plate when in working condition had to be met. In working condition, the plate is fastened securely essentially giving it a fixed boundary condition along the bottom of the cylinder.

Therefore, the entire assembly was attached to a 317.5 mm diameter, 19 mm thick aluminum plate. It was secured using 6.4 mm bolts through twelve evenly spaced holes drilled in the fixture. For use with a small 444N modal shaker, a center hole was tapped and drilled to allow for a stinger to be inserted to excite the assembly. As multiple specimens were under investigation it is imperative to be cognizant of the fact that all dimensions are nominal and subject to variation. Another means of variation that can arise from test specimen to test specimen is the fact that the welding process of the plate into the can may induce residual stresses into the system. Finally, it was originally assumed that the plate assembly was entirely geometrically symmetric however, some asymmetry was expected.





**Figure 2: Perforated plate welded into supporting cylinder**

### **3. Linear Analysis of Circular Perforated Plates**

While the plate will prove to be nonlinear in nature it is useful to ascertain the linear region of the plates' motion for comparison of natural frequencies and mode shapes as well as for updating the FEM in the same linear region. Even though a finite element model will be used for comparison, it is important that the correct boundary conditions be used and one of the best ways to verify the boundary conditions is to use an analytical model. If the natural frequencies and mode shapes of the analytical model match within reason that of the numerical model and experimental data, then the boundary conditions of the numerical model are assumed to be correct. In "Vibration of Continuous Systems" by Rao [13], he begins the analysis of circular plates by looking at

an infinitesimal element of a plate in polar coordinates. To simplify his model but still allow it to be useful, a series of general assumptions are made and are as follows. Firstly, that the thickness of the plate  $h$  is small compared to any other dimensions of the plate. Rao states that a general rule of thumb for determining if the thickness is small compared to other dimensions is that the ratio between the two should be less than 1:10; but depending on the application may be as much as 1:20. Secondly, while the plate is bending it experiences no strain along the middle surface. Thirdly, that the plane sections remain plane and do not warp in any manner. Fourthly, since the relative thickness of the plate is small the normal stresses in the transverse direction are ignored. Fifthly, that the deflections of the plate at any point are small. Lastly, that shear and rotary inertia are ignored. With these assumptions the equations of motion for a circular plate are derived based off the free body diagrams for dynamic equilibrium of the element in Figure 3

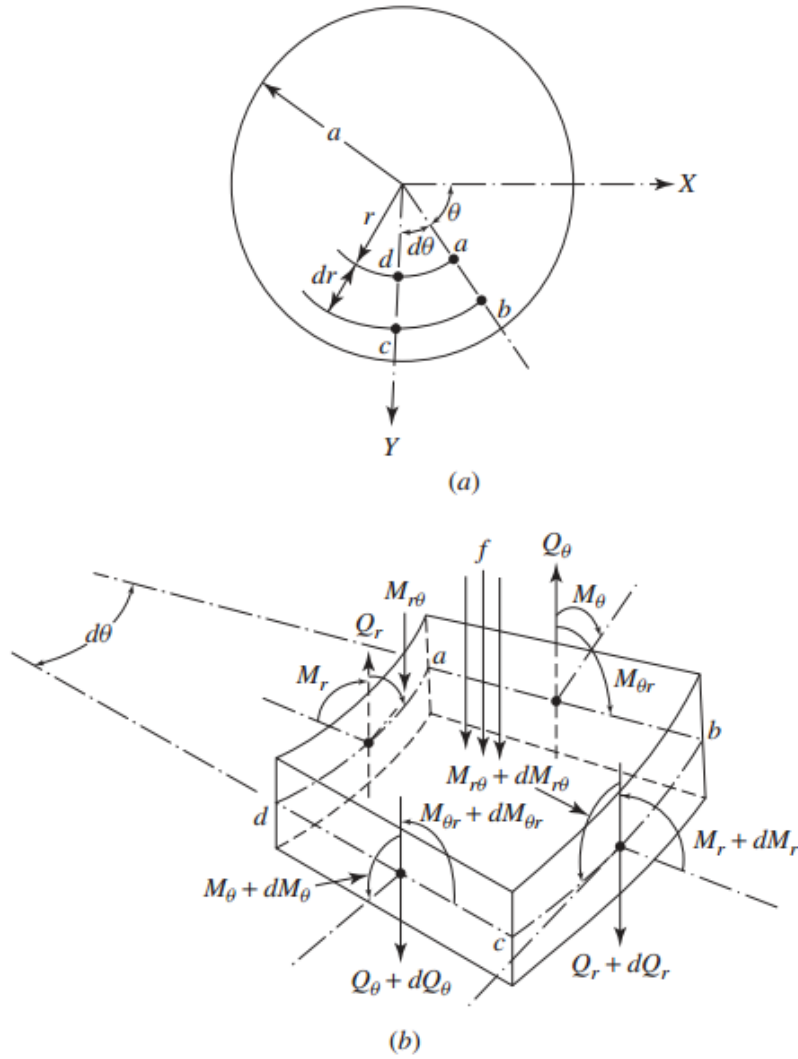


**Figure 3: (a) Polar coordinates of plate (b) Free body diagram of plate element [13]**

where Rao defines the radial moment of the plate as  $M_r$ , the tangential moment as  $M_\theta$ , the twisting moments as  $M_{r\theta}$  and  $M_{\theta r}$ , and the transverse shear forces as  $Q_\theta$  and  $Q_r$ . Summing the moments about the tangential direction ( $\theta$ ), Rao produces the moment equilibrium equation in Equation 1. It is important to note that the subscripts of the moments and shear forces represent their directions.

$$\frac{\partial M_r}{\partial r} + \frac{1}{r} \frac{\partial M_{r\theta}}{\partial \theta} + \frac{M_r - M_\theta}{r} - Q_r = 0 \quad (1)$$

Similarly Rao derives the moment equilibrium equation about the radial direction ( $R$ ) in Equation 2.

$$\frac{\partial M_{r\theta}}{\partial r} + \frac{1}{r} \frac{\partial M_\theta}{\partial \theta} + \frac{2}{r} M_{r\theta} - Q_\theta = 0 \quad (2)$$

Using Newtons' second law to equate the forces in the  $z$  direction to the inertia forces in the  $z$  direction, Rao acquires Equation 3, where the transverse displacement is defined as  $\omega(r, \theta, t)$ .

$$\frac{\partial Q_r}{\partial r} + \frac{1}{r} \frac{\partial Q_\theta}{\partial \theta} + \frac{Q_r}{r} + f - \rho h \frac{\partial^2 \omega}{\partial t^2} = 0 \quad (3)$$

In the above equation for the force equilibrium,  $f$  is defined as the transverse force applied to the element in the  $z$  direction,  $\rho$  is the volume density, and  $h$  is the height of the element.

Rao then proceeds to create a single equation of motion in terms of  $M_r$ ,  $M_\theta$ , and  $M_{r\theta}$  by combining Equations 1-3. From there he creates the final transverse equation of motion for a circular plate in Equation 4 by substituting the moment resultants in terms of the transverse displacement  $\omega$ .

$$D \nabla^4 \omega + \rho h \frac{\partial^2 \omega}{\partial t^2} = f \quad (4)$$

This may also be expressed as,

$$D \left( \frac{\partial^4 \omega}{\partial r^4} + \frac{2}{r} \frac{\partial^3 \omega}{\partial r^3} - \frac{1}{r^2} \frac{\partial^2 \omega}{\partial r^2} + \frac{1}{r^3} \frac{\partial \omega}{\partial r} + \frac{2}{r^2} \frac{\partial^4 \omega}{\partial r^2 \partial \theta^2} - \frac{2}{r^3} \frac{\partial^3 \omega}{\partial r \partial \theta^2} + \frac{4}{r^4} \frac{\partial^2 \omega}{\partial \theta^2} + \frac{1}{r^4} \frac{\partial^4 \omega}{\partial \theta^4} \right) + \rho h \frac{\partial^2 \omega}{\partial t^2} = f(r, \theta, t) \quad (5)$$

In the above mentioned equations  $\nabla$  is the biharmonic operator and  $D$  is defined as the flexural rigidity of the plate and can be expressed as  $D = Eh^3 / (12(1-\nu^2))$ ; where  $E$  is Young's modulus and  $\nu$  is Poisson's ratio of the plate.

In order to obtain the mode shapes and natural frequencies of the circular plate, the eigenvalue problem must be found and solved for the correct boundary conditions. Using the assumption that the solution can be separated in space and time,

$$\omega(r, \theta, t) = W(r, \theta) T(t) \quad (6)$$

the eigenvalue problem for free boundary conditions of a circular plate can then be found by the separation of variables from Equation 4,

$$\frac{d^2 T(t)}{dt^2} + \omega^2 T(t) = 0 \quad (7)$$

$$\nabla^4 W(r, \theta) - \lambda^4 W(r, \theta) = 0 \quad (8)$$

Where

$$\lambda^4 = \frac{\rho h \omega^2}{D} \quad (9)$$

Rao then proceeds to use the separation of variables technique to solve the differential equation to obtain the general eigenvalue problem in terms of Bessel functions as seen in Equation 10.

$$W(r, \theta) = [C_m^{(1)} J_m(\lambda r) + C_m^{(2)} Y_m(\lambda r) + C_m^{(3)} I_m(\lambda r) + C_m^{(4)} K_m(\lambda r)](A_m \cos m\theta + B_m \sin m\theta), \text{ for } m=0,1,2,\dots \quad (10)$$

Where  $J_m$  and  $Y_m$  are Bessel functions of the order  $m$  of the first and second kind, respectively.  $I_m$  and  $K_m$  are considered hyperbolic Bessel functions or modified Bessel functions of the order  $m$  of the first and second kind, respectively. Also in the above equation is a series of constants,  $C_m^{(1)}, \dots, C_m^{(4)}, A_m, B_m$ , and  $\lambda$  that are entirely dependent on the boundary conditions of the plate.

To obtain the shape function for the circular perforated plate, we assume the fact that the weld on the cylinder creates a fully clamped boundary condition. Neglecting the small curvature on the edge of the plate where it connects to the cylindrical can, the boundary conditions in terms of  $W(r, \theta)$  then becomes,

$$W(a, \theta) = 0 \quad (11)$$

$$\frac{\partial W}{\partial r}(a, \theta) = 0 \quad (12)$$

where  $a$  is outer radius of the plate. Using the boundary conditions and knowledge of the solutions of Bessel functions, Equation 10 then becomes a practical shape function for the circular perforated plate and is shown in Equation 13.





$$W(r, \theta) = [J_m(\lambda r) - \frac{J_m(\lambda a)}{I_m(\lambda a)} I_m(\lambda r)] (A_m \cos m\theta + B_m \sin m\theta), \quad (13)$$

for  $m=0,1,2,\dots$

The natural frequencies are found by solving for the eigenvalues using the relations between Equations 12 and 13; the final form of which can be seen in Equation 14 where  $\omega_{mn}$  is the natural frequency and  $\lambda_{mn}$  are the eigenvalues. The indices  $m$  and  $n$  help describe the mode shape.  $m$  is the number of nodal diameters and  $n$  is the number of nodal circles not including the boundary for each mode shape.



$$\omega_{mn} = \lambda_{mn}^2 \left( \frac{D}{\rho h} \right)^{1/2} \quad (14)$$

The shape function reveals that for a circular plate with clamped boundary conditions the mode shapes begin to arrange themselves as seen in the six figures that are taken from [14] in Table 1. Also the first 11 natural frequencies calculated using Equation 14 and their corresponding mode shapes descriptions can be found in Table 1

Mode Number	Natural Frequency (Hz)	Mode Shape Description
1	201.13	One Nodal Circle 
2	418.40	One Nodal Diameter 
3	686.44	One Nodal Circle and Two Nodal Diameters 
4	782.67	Two Nodal Circles 

**Table 1: Theoretical natural frequencies and mode shapes for a clamped circular plate**



Mode Number	Natural Frequency (Hz)	Mode Shape Description
5	1004.5	Three Nodal Diameters and One Nodal Circle 
6	1196.9	One Nodal Diameter and Two Nodal Circles 
7	1371	Four Nodal Diameters and One Nodal Circle
8	1663.7	Two Nodal Diameters and Two Nodal Circles
9	1753.5	Three Nodal Circles
10	1785.7	Five Nodal Diameters and One Nodal Circle
11	2184.5	Three Nodal Diameters and Two Nodal Circles

**Table 1 (Continued): Theoretical natural frequencies and mode shapes for a clamped circular plate**

### 3.1 Finite Element Model

The original finite element model (FEM) of the plate that was created, modeled the plate as a flat solid circular plate with curved edges and with the nominal geometries

listed earlier in the test specimen section of this thesis. However, the FEM does not include the cylinder that the plate is welded into. Instead boundary conditions identical to the theoretical boundary conditions of a fixed or clamped plate were added. Due to the assumption of the plate not having initial curvature, with the exception of the curved edges, the original plate will be referenced in this thesis as finite element model with no initial curvature (FEM-NIC). The main difference between the FEM-NIC and the actual test specimen is the fact that the perforations were omitted in the FEM. In order to keep the perforations in the model, a very detailed mesh would have to have been generated. However, because such plates with perforations are being seen more and more in various applications; many finite element analysis techniques have been generated to reduce the time and cost of creating such a model. One such technique is presented in a study completed by Mali and Singru [15], where the authors successfully model a rectangular plate with a rectangular array of circular perforations by substituting the circular perforations with equivalent square perforations in order to use unit step functions. They then use the Rayleigh-Ritz method to determine the fundamental frequencies. Similar to this work is the work of Jhung and Jo [16], who endeavor to prove that plates with triangular or square perforation patterns may be modeled by an equivalent plate with no perforations. Their technique is successful due to the fact that they adjust the elastic modulus and density to what is described as an effective modulus and effective density that properly defines the reduced mass and volume of the plate. Using the work detailed by Jhung and Jo [16] for triangular perforations, the FEM-NIC model's original Young's modulus and density for 409 stainless steel were altered to an effective Young's modulus of 1.68 GPa and an effective density of 5120 kg/m<sup>3</sup>. While the effective density was

thought to be quite accurate due to its sole dependence on geometry of the triangular perforations; the effective Young's modulus is in question due to its dependence on the stiffness of the material. The stiffness was difficult to ascertain because of the orthotropic nature that the perforations introduced and was therefore thought to be inaccurate. Also, there are thought to be numerous conditions upon which stresses were added to the plate making the chosen effective modulus suspect. These stresses could have been added with the addition of the perforations in the plates or from the fact that the geometry of the perforations is not uniform throughout. Another possibility for residual stress to be added to the plate is when the plate is bent into its final shape.

Figure 4 shows the meshed model from which the nonlinear normal modes of vibration were computed for comparison. Each mode of vibration had its own reduced order model using the Implicit Condensation method [17,18,19] and the reduced ordered models were integrated using Peeters, Kerschen, et al [20] NNM Cont. MATLAB program to compute the nonlinear normal modes of vibration. The combination of the Implicit Condensation method and the NNM Cont. MATLAB program were shown to estimate the backbone curves of the NNMs of a geometrically nonlinear beam with great results in [8,9]. As a result it was thought that the methods used in those studies would give an accurate approximation of the NNMs of the nonlinear plate in this thesis.

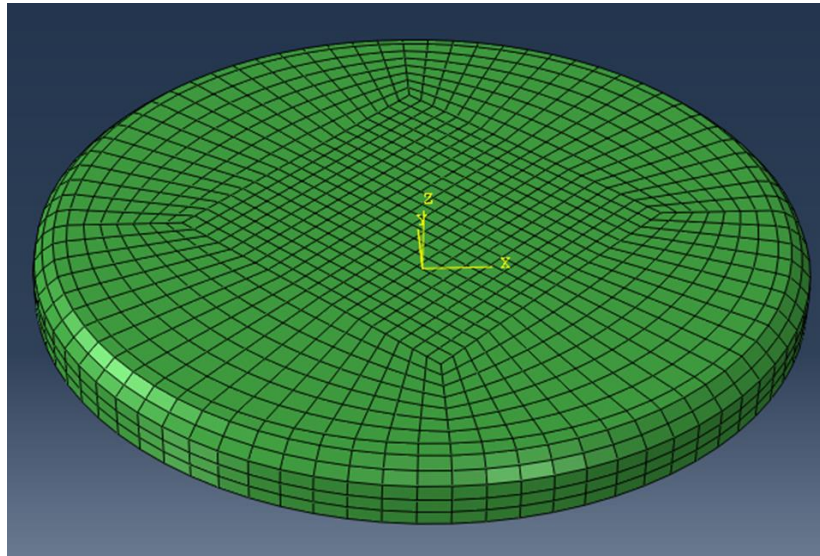


**Figure 4: Mesh of Perforated Plate Model FEM-NIC**

### **3.2 Roving Hammer Tests**

To compare to the theoretical and numerical natural frequencies and mode shapes in the linear region of vibration, a roving hammer test of the circular perforated plate was performed. A roving hammer test consists of exciting the structure under consideration by striking it sequentially at predetermined points with a modal hammer, while measuring the response on the structure. The circular perforated plate was given 37 predetermined impact points by creating a 50 mm square grid on the surface. The responses of the plate were measured using accelerometers at the locations discussed in the nonlinear analysis section of this thesis in Table 5. An extra point was selected at the location of accelerometer C; bringing the total number of impact points to 38. Initial tests showed that the plate behaved nonlinearly for small excitations and as a result a small modal hammer, seen in Figure 5; was chosen to keep the plates responses linear.

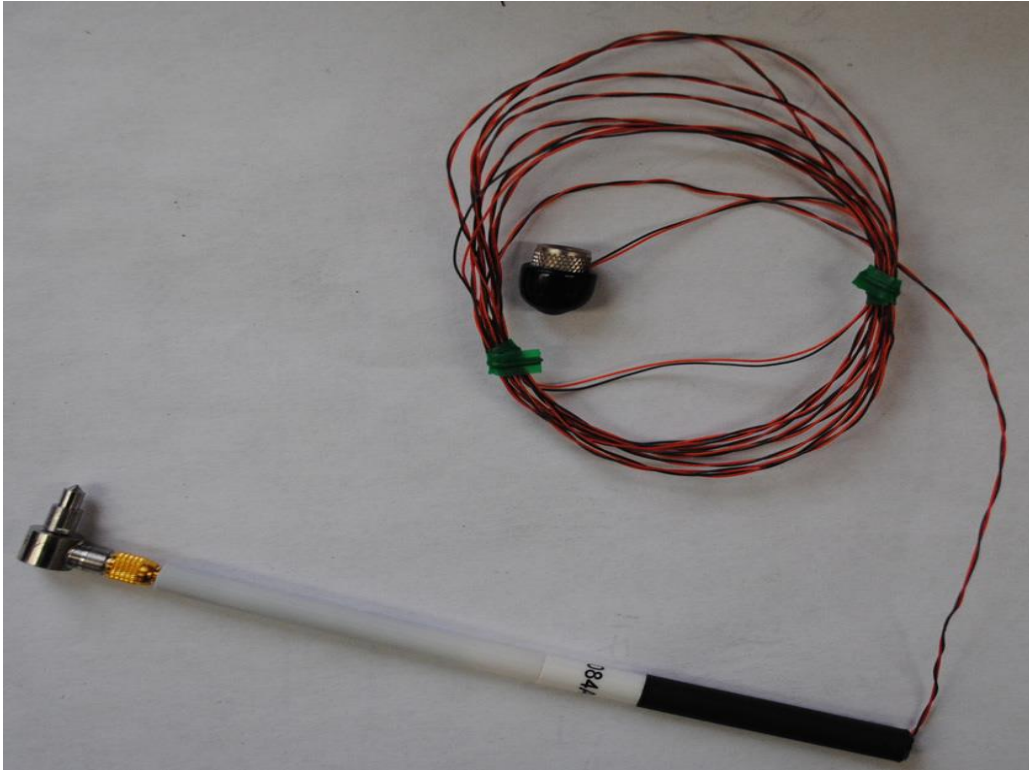


**Figure 5: Modal Hammer PCB 086E80**

During testing, the coherence between the accelerometers and the modal hammer, as well as the transfer functions were recorded to verify that the response remained linear and that the proper modes of vibration were excited after each hammer impact. Each location on the grid was impacted 3 times and averaged. After data was properly acquired at each point of interest on the plate, the natural frequencies and mode shapes were derived from the algorithm of mode isolation (AMI) [21]. The results of which can be seen in Tables 2 and 3.

### **3.3 Comparison of the Linear Analysis of the Circular Perforated Plate**

In order to properly compare the natural frequencies of the analytical and numerical models, along with the data obtained experimentally, the mode shapes must be

compared as well. If the natural frequencies are similar but the mode shapes for those two frequencies are different then the two modes are in actuality two entirely different modes. Using Equation 13 and inserting the locations of the 38 points from the roving hammer test, the theoretical mode shapes can be modeled for comparison with the experimental and the numerical mode shapes. This is accomplished by using the Modal Assurance Criterion, or MAC value, which is a statistical indicator that runs from 0 to 1 with 1 being a perfect match.

In Table 2, the natural frequencies of the theoretical analysis and the natural frequencies from the FEA model are compared. It became apparent while developing the mode shapes from the numerical model that repeating modes occurred at or near the same natural frequency. These repeated modes turned out to be symmetric modes, and in order to match the symmetric modes in the numerical model with that of the theoretical model; the theoretical model was rotated by 45 degrees, -45 degrees, and 22.5 degrees. The combination of rotated and non-rotated theoretical models produced a very good series of MAC values with the lowest value being only 0.895. Therefore, it can be concluded that the correct boundary conditions were indeed modeled in the numerical analysis and that they are fixed or clamped and not that of simply supported or simply supported with an elastic edge.

Theoretical Mode Number	$f_n$ , Theoretical (Hz)	FEM 2-NIC Mode Number	$f_n$ , FEM 2-NIC (Hz)	% Error	MAC Values
1	201.129	1	204.8	1.83	0.993
2	418.40	2	424.88	1.55	0.986
2	418.40	3	424.88	1.55	0.986
3	686.44	4	701.64	2.21	0.985
3	686.44	5	702.93	2.40	0.976
4	782.67	6	803.68	2.68	0.971
5	1004.5	7	1033.7	2.91	0.899
5	1004.5	8	1033.7	2.91	0.899
6	1196.9	9	1226.1	2.44	0.971
6	1196.9	10	1226.1	2.44	0.971
7	1371	11	1421.7	3.70	0.960
7	1371	12	1424	3.87	0.999
8	1663.7	13	1713.7	3.01	0.982
8	1663.7	14	1725.7	3.73	0.950
9	1753.5	15	1817.4	3.64	0.959
10	1785.7	16	1872.1	4.84	0.957
10	1785.7	17	1872.1	4.84	0.957
11	2184.5	18	2271.3	3.97	0.895
11	2184.5	19	2271.3	3.97	0.895

**Table 2: Analytical natural frequencies and their mode numbers compared to numerical natural frequencies and their mode numbers.**

Table 3 similarly compares the theoretical natural frequencies with the extracted natural frequencies from the experimental hammer test. The symmetric modes were again observed in the experimental testing and the same series of rotations were applied to the theoretical model to attempt to match all the mode shapes. However, even with the rotation the mode shapes did not always produce a good MAC number. Modes 2, 14, 15, 16 and 18 of the experimental data all have MAC number less than 0.80 and span as low as 0.442. Unlike the theoretical and numerical comparison, the theoretical and

experimental natural frequencies are quite different even with a good MAC value for the mode. After the first mode it can be seen that all the subsequent modes occur at lower frequencies than the theoretical model. One likely reason for the lower natural frequencies is the inclusion of in plane stresses in the experimental data. If you recall, in plane stress was excluded by Rao in developing his shape and natural frequency equations and is also excluded in the finite element analysis. It can be concluded from Table 3 that while the mode shapes match fairly well for the most part the natural frequencies extracted from the experimental data are consistently lower than the theoretical natural frequencies with a max error of the computed natural frequencies being 34.53 percent. Therefore, the model that was used is not completely accurate and will most likely not produce the proper NNMs for comparison. In order to correct the disparity, the model will need to be updated by investigating whether or not the residual stresses are in fact the deconstructive factor.



Theoretical Mode Number	$f_n$ , Theoretical (Hz)	Experimental Mode Number	$f_n$ , Experimental (Hz)	% Error	MAC Values
1	201.129	1	205.91	2.38	0.976
2	418.40	2	328.35	21.52	0.679
2	418.40	3	348.83	16.63	0.949
3	686.44	4	489.44	28.70	0.927
3	686.44	5	510.93	25.57	0.923
4	782.67	6	554.49	29.15	0.911
5	1004.5	7	698.27	30.49	0.966
5	1004.5	8	699.76	30.34	0.856
6	1196.9	9	813.81	32.01	0.932
6	1196.9	10	826.26	30.97	0.926
7	1371	11	922.04	32.75	0.969
7	1371	12	939.09	31.50	0.952
8	1663.7	13	1089.48	34.51	0.938
8	1663.7	14	1102.53	33.73	0.777
9	1753.5	15	1176.23	32.92	0.594
10	1785.7	16	1190.78	33.31	0.442
10	1785.7	17	1200.29	32.78	0.852
11	2184.5	18	1430.13	34.53	0.658
11	2184.5	19	1434.78	34.32	0.870

**Table 3: Analytical natural frequencies and their mode numbers compared to experimental natural frequencies and their mode numbers.**

The comparison between the FEA model and the experimental data is shown in Table 4 and again the natural frequencies of the experimental data are consistently lower than the natural frequencies of the FEA model. This suggests that the effective modulus used to represent the perforations in the test specimen is too high. It can also be concluded from Table 4 that the mode shapes match fairly well with a couple of exceptions. The MAC values associated with the mode shapes have a large span of values from 0.988 to 0.500. The comparison of natural frequencies in Table 4 also produces the

highest percent error with a maximum value of 37.03 percent. The only two modes that did not produce a good enough mode shape to conclude that the mode from the numerical analysis matched a mode from the experimental analysis were modes 15 and 16. Upon graphing the mode shapes to observe them, it was found that the shapes seemed similar but something unexpected was occurring. In the experimental data, it appeared that there was an inclusion of nodal diameters that were not expected and did not appear in the numerical or theoretical data. This could mean that these two modes are higher order modes that were not calculated in the numerical or theoretical cases but it is difficult to say and therefore it is unknown why the mode shapes do not match for these two instances.

FEM 2-NIC Mode Number	$f_n$ , FEM 2-NIC (Hz)	Experimental Mode Number	$f_n$ , Experimental (Hz)	% Error	MAC Values
1	204.8	1	205.91	0.54	0.988
2	424.88	2	328.35	22.72	0.893
3	424.88	3	348.83	17.90	0.880
4	701.64	4	489.44	30.24	0.915
5	702.93	5	510.93	27.31	0.915
6	803.68	6	554.49	31.01	0.900
7	1033.7	8	698.27	32.45	0.932
8	1033.7	7	699.76	32.31	0.924
9	1226.1	10	813.81	33.63	0.921
10	1226.1	9	826.26	32.61	0.913
11	1421.7	11	922.04	35.15	0.953
12	1424	12	939.09	34.05	0.952
13	1713.7	13	1089.48	36.43	0.934
14	1725.7	14	1102.53	36.11	0.909
15	1817.4	15	1176.23	35.28	0.590
16	1872.1	16	1190.78	34.48	0.500
17	1872.1	17	1200.29	35.89	0.833
18	2271.3	18	1430.13	37.03	0.795
19	2271.3	19	1434.78	36.83	0.888

**Table 4: Numerical natural frequencies and their mode numbers compared to experimental natural frequencies and their mode numbers.**

#### **4. Experimental Setup for Small Shaker**

The initial tests for the exhaust plate assembly were to be conducted on a small modal shaker. This shaker was assumed to allow the plate to act in a linear range to compare with the nonlinear behavior of the plate. The model of the shaker that was chosen was a Ling Dynamics LMT-100. This particular shaker was capable of generating a maximum sinusoidal forcing amplitude of 444 Newtons (100 lbf). It was decided that the optimum method to excite the modes that will most likely be seen in operation would

be to employ a base excitation. As aforementioned in a previous section, a hole was tapped and drilled into the fixture plate that would allow a 5 mm stinger to excite the assembly. The plate assembly was to be tested vertically and therefore, the assembly was hung via four bungee cords from a lateral excitation stand. Four extended bolts and nuts were used to attach the assembly to the bungee cords.

In the center of the fixture plate was placed a 3 axis accelerometer (accelerometer A), to initially try to control the forcing amplitude of the shaker. Two other accelerometers were placed on the exhaust plate at vital points to measure the response of the plate. These accelerometers locations and sensitivities can be viewed in Table 5. Accelerometer B was placed at the center of the plate to help identify modes that consisted of nodal circles while accelerometer C was placed at exactly one third the radius of the plate from the center to assist in identifying modes with nodal diameters. In anticipation of low forces and frequencies, all of the accelerometers were fixed to their respective plates using wax. The data acquisition system that was used for this study was the Data Physics® ABACUS hardware with SignalCalc Mobilyzer software developed by Data Physics. The ABACUS system was used to drive the shaker as well as to acquire the measured results. The SignalCalc Mobilyzer software computed the steady state response frequency as well as the amplitude at each frequency.

Accelerometer	Location of accelerometers on test set-up	Type	Sensitivity (mV/g)
A	Center of fixture plate	3 axis IEPE TEDS	106.2
B	Center of exhaust plate	ISOTRON 25B	4.67
C	One third the radius from the center of the exhaust plate	ISOTRON 25B	5.30

**Table 5: Location type and sensitivities of accelerometers used in stepped-sine tests**

To begin with, a closed loop, sine sweep excitation using Data Physics SignalStar Vector II was attempted to acquire the nonlinear frequency response. Wide sine sweeps of both increasing and decreasing frequency at prescribed forcing amplitudes was endeavored to obtain the forced response frequencies (FRFs) of the plate. While sweeping in either direction the controller was attempting to use accelerometer A to maintain constant forcing amplitude. Once a sweep was completed at single forcing amplitude, it would be increased by a predetermined interval and another sweep would be completed. However, as the frequency approached resonance the control software would have to adjust the input very quickly in order to avoid perturbing the system; causing it to move off the resonance and possibly onto a co-existing low amplitude branch of the NNM. Therefore, the swept sine measurement technique proved lacking in that it could

not stay on the same forcing amplitude as it approached resonance. This caused the FRF to have responses not characteristic with the desired forcing amplitudes and therefore would not give proper backbone curves to estimate the NNM from. In addition, the acquired data from the swept sine measurements would have to be post processed to estimate the amplitude of the response and the phase at each frequency. It was then determined that a stepped-sine test would produce more readily available and reliable data to extract the NNMs from.

As the data collection veered from a controlled sine sweep to a stepped-sine test, it was thought to be beneficial to step through each mode individually instead of sweeping through a large bandwidth with multiple modes using the NNM force appropriation techniques previously discussed. The natural frequencies of the various modes were discovered in the linear testing of the plate. What remained unknown was which modes would see the highest responses in operation. Therefore, the leading test on the exhaust plate was to experimentally determine the magnitude of the responses of the modes. To achieve this, a burst random analysis was completed over a bandwidth of 0-1000 Hz. In order to ensure that the data collected for the burst random analysis was precise, the results were averaged ten times within the program and the results of the burst random analysis can be seen in Figure 6.

It is evident from the burst random analysis observed from accelerometer B that the first mode has a high response that will most likely appear in operation. The next two modes that are observed from the burst random analysis occur between 300 and 400 Hz. The low magnitude responses that were seen in both accelerometers means that in

operation they are not likely to be excited and as a result they were not investigated in this study. In addition to this, the roving hammer tests suggests that these two modes, as well as the next two modes that occur around 500 Hz; are in actuality anti-symmetric modes with nodal diameters as seen in Table 1. The second pair of anti-symmetric modes, modes 4 and 5; however, will be observed due to the high response seen in accelerometer C. The sixth mode of vibration at around 570 Hz experiences another large response from accelerometer B. This is consistent with the linear analysis in Table 1, where the mode shape consists of nodal circles resulting in a higher response from accelerometer B. As a result of the high responses observed and assuming that all other modes behave linearly, modes 1, 4, 5, and 6 were chosen as modes that their respective NNMs could be extracted from.

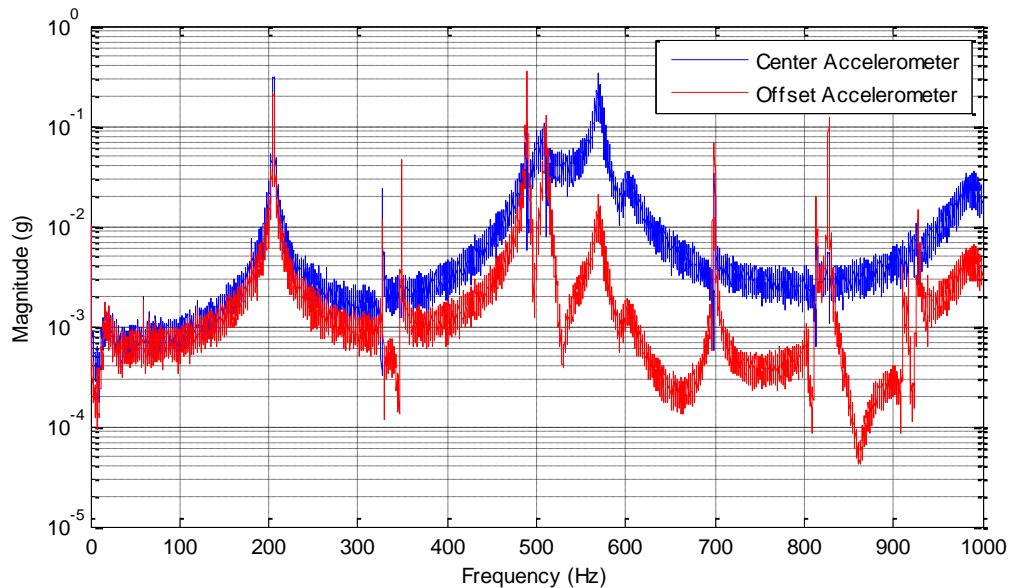


**Figure 6: Burst random analysis of Cummins perforated plate**

SignalCalc Mobilyzer was now the software used with the Data Physics controller in order to operate the stepped-sine feature of the data acquisition hardware. With the current setup of a tri-axial accelerometer in the center of the fixture plate and two accelerometers to measure the response on the exhaust plate, a semi-closed loop control was attempted to ensure that each individual frequency response function (FRF) would stay on its specific branch. It was imperative that each FRF remained on its specific branch as a base characteristic of NNMs is its frequency energy dependence. If the applied forcing amplitude was suddenly changed around resonance, then the response may jump to a lower or higher branch of the NNM. Thus, when the NNM would be extracted the backbone curve made from the FRFs, which describes the NNM, would be incorrect.

As testing commenced it was apparent that simply using accelerometers to control the forcing amplitude was insufficient and a force transducer was thought to provide the best solution. A Piezotronics PCB208C04 force transducer with a 22mV/N sensitivity was mounted between the stinger of the shaker and the fixture plate and the complete experimental setup for stepped sine measurements can be viewed in Figure 7. With the addition of the force transducer, a quasi-closed loop function of SignalCalc was now used to control the forcing amplitude to a desired input force; ensuring that the FRF would now stay on the desired branch of the NNM around resonance.



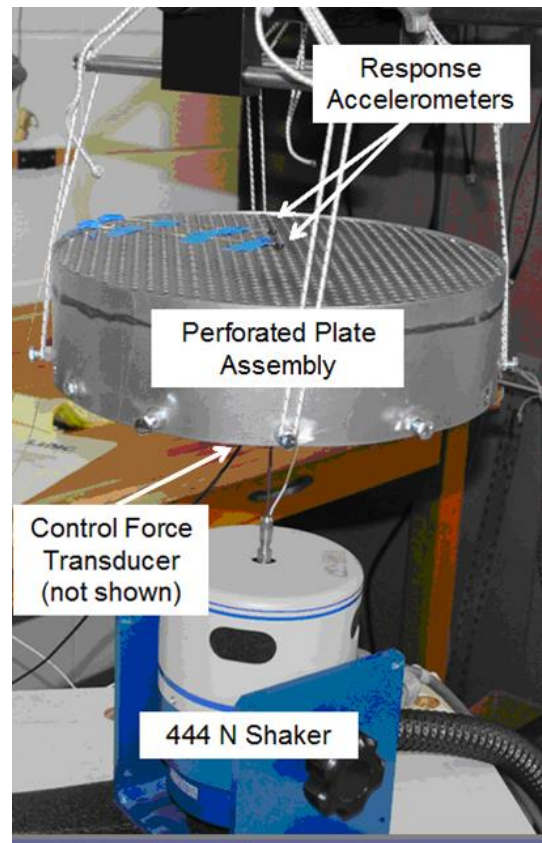


**Figure 7: Experimental Setup**

With the inclusion of the force transducer the stepped-sine function of SignalCalc now operated by forcing the shaker at a desired frequency until steady state was achieved upon which it would step up in frequency by a prescribed increment. The software monitored the forcing amplitude and the voltage of the shaker at each step and if the amplitude did not match the input value then the program would dwell at that specific frequency and adjust the forcing amplitude until it returned to within 10% of the target value. Once steady state was achieved at the correct forcing amplitude the program continued stepping as normal.

For each individual mode on the 100 lbf modal shaker, a small bandwidth was selected of only 10 Hz with a 100 steps, resulting in a frequency step size of only 0.1 Hz. The frequency was stepped up and back down at each individual forcing amplitude multiple times to confirm the FRF being recorded and the boundary conditions of the test were not changing. The increment at which the forcing amplitude was increased was dependent on the particular mode being investigated. The first mode appeared to have a more drastic change in peak response frequency and as a result a smaller increment of 0.1 lbf was used. The fourth, fifth, and sixth modes appeared to be more linear and therefore an increment of 1.0 lbf was used instead. The first forcing amplitude used for all tests was chosen to be as low as the shaker would allow steady state in order to attempt to observe the change from the linear range to the nonlinear range. As a result the force increments are not equally spaced.

Around resonance it wasn't uncommon for the forcing amplitude to either increase or decrease by as much as a factor of 2 and therefore substantial effort was made to assure that the software would dwell long enough to obtain the correct forcing amplitude at steady state. Depending on the shaker and the mode being assessed, there could be multiple solutions to keep the forcing amplitude that SignalCalc used as its control constant. One solution is simply to increase the tolerances allowed for the forcing amplitude. Although this is not ideal, for certain situations it may prove to be the only option. Another solution is to adjust the settling time for the program to dwell at each individual frequency for one iteration. This can be accomplished by setting the settling time to either cycles or seconds and entering a manually determined amount that you wish the program to wait to settle at a single iteration of every frequency step. In this

thesis the forcing amplitude was kept within tolerance by adjusting the number of iterations that the algorithm would attempt at each frequency while keeping the settling time for each iteration automatic. However, with some practice and patience the correct number of iterations was discovered and numerous forcing amplitudes were now quite simple to acquire at steady state.

#### **4.1 First Mode of Vibration on Small Shaker**

The first mode of vibration for the exhaust plate examined occurred at 205.36 Hz in the hammer test and a bandwidth of 10 Hz was chosen to step through around this frequency. It was imperative that the phase angle at steady state was captured to validate that the NNM had been achieved according to the phase lag quadrature criterion.

Therefore, a small step size was considered the best option and 100 data points were taken, resulting in a data point at every 0.1 Hz. Using the quasi-closed loop algorithm in the shaker control software, the force stayed within 10% of the required forcing amplitude. Figure 8 displays the results of the stepped sine measurements starting at a forcing amplitude of 0.1 lbf to a maximum 3.0 lbf by increments of 0.1 lbf, resulting in 30 subsequent FRF curves for stepping up in frequency and stepping down in frequency to extract the NMM from. There was a desire to continue stepped sine measurements past 3.0 lbf, yet just above this limit the plate would begin to oscillate from side to side and the system would never reach a steady state either stepping up or stepping down in frequency. It is thought that at this forcing amplitude the stinger from the shaker to the plate experiences some sort of bending causing the plate to begin to oscillate laterally. The initial starting amplitude of 0.1 lbf was chosen to attempt to convey the linearity of the exhaust plate under consideration, yet it is apparent from stepping up and stepping

down in frequency that the FRFs even at that low forcing amplitude are not entirely linear and this can be seen in Figure 8 (c) and (d) respectively. Examining Figure 8 reveals that the plate at the first mode of vibration experiences a softening nonlinearity from the peak moving towards lower frequencies as the forcing amplitude increases. The maximum frequency shift of the plate is 5.3 Hz and can be found on Figure 8 (d) where the program is stepping down in frequency. This difference in frequency is not however observed in Figure 8 (c) where the program is stepping up in frequency. It is thought that this is a result of the FRF beginning closer to the NNM around resonance when stepping down and therefore remains on the NNM longer until it reaches its maximum response, upon which it experiences what is commonly known as the jump phenomena. The jump phenomena is when the response of the system suddenly and drastically decreases or increases in amplitude for a small increase or decrease in the excitation frequency applied to the system.

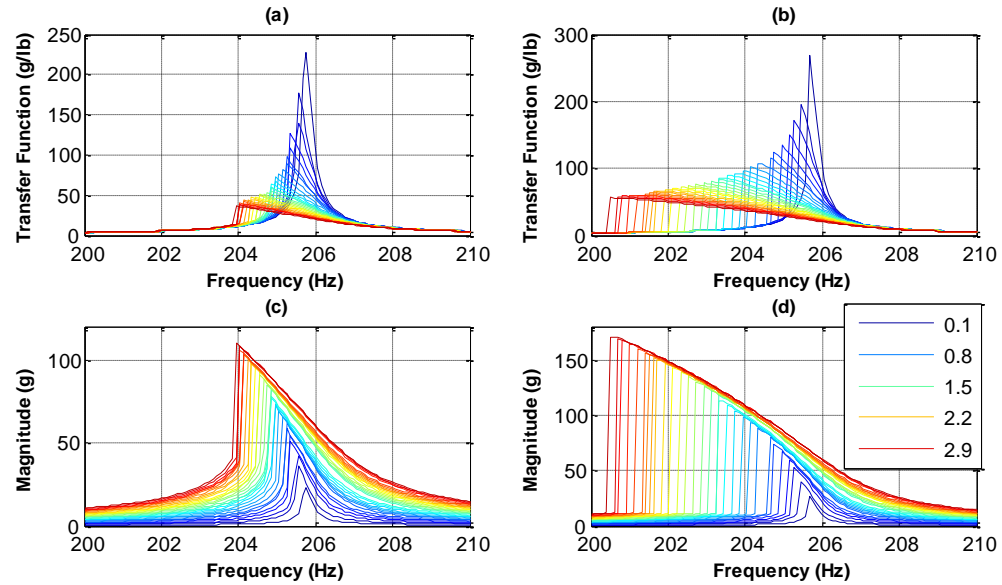


**Figure 8: Transfer function of first mode stepping (a) up (b) down in frequency.**

#### **FRFs of first mode stepping (c) up (d) down in frequency**

According to the phase lag quadrature criterion previously discussed, when a phase shift of 90 degrees occurs between the force and the acceleration then resonance has been achieved and that point becomes a piece of the backbone of the NNM for that mode of vibration. SignalCalc allows us to track the phase angle of the transfer function for the first mode of vibration as the frequency changes and this can be seen in Figure 9. The data points are where the phase was recorded at or nearest 90 degrees and are represented by the markers. It can clearly be seen that in Figure 9 (b), when the program is stepping down, or rather when it theoretically conforms to the NNM earlier; the collected data points are very near 90 degrees phase angle with only a couple true outliers. In contrast, when the software steps up in frequency, the data points do not occur

anywhere close to the 90 degree phase angle. This is common for nonlinear systems with a softening effect as the jump phenomena causes the response to quickly pass through the 90 degrees phase point.

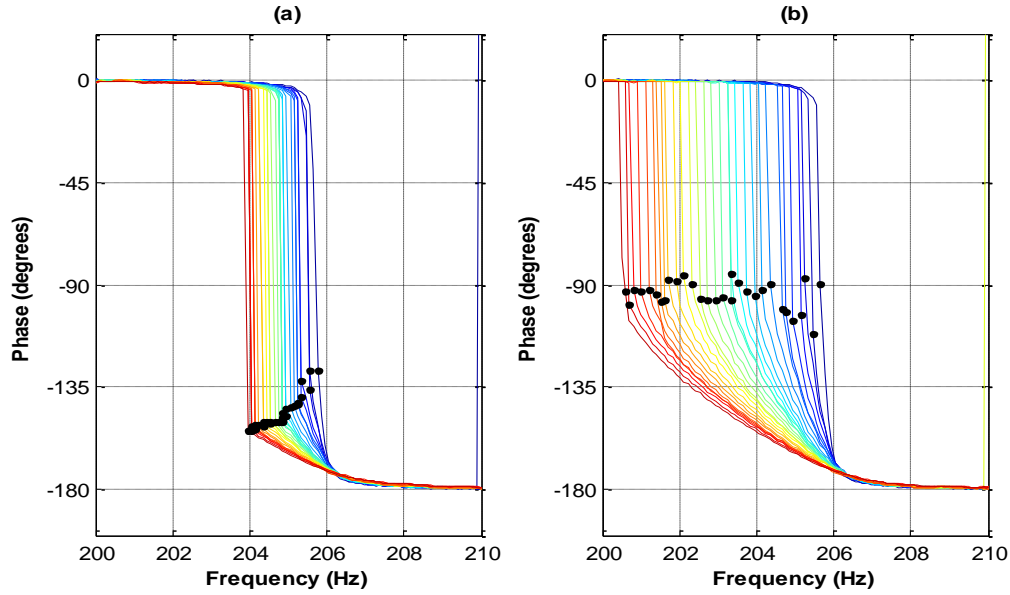


**Figure 9: Phase lag of the first mode (a) stepping up (b) stepping down in frequency.**

**Markers indicate points of the first mode from which the NNM was extracted.**

## 4.2 Fourth, Fifth, and Sixth Modes of Vibration on Small Shaker

In order to legitimize the method used to extract the NNMs from the exhaust plate, more than simply the first mode of vibration must be analyzed. Observing different modes of vibration from the same system provide critical insight into how the method of stepped-sine measurements to extract an NNM performs with different mode shapes and response amplitudes, as well as various levels of nonlinearity. Replicating the test procedure described in the first mode of vibration as well as the experimental test setup,

modes 4, 5, and 6 were analyzed to determine if the stepped-sine approach to extracting NNMs would differ at all or possibly produce better results.

The fourth and fifth modes of vibration are closely spaced anti-symmetric modes consisting of nodal diameters as can be seen in Table 1. Since closely spaced modes commonly have some sort of interactions between them, curiosity arose as to how the FRFs and NNMs would evolve as energy increased. If the nonlinearity seen in the first mode persisted then it was hypothesized that most likely some sort of bifurcation or internal resonances would be seen. However, stepped sine measurements of both increasing and decreasing frequency were conducted and no such interactions were seen. The forcing amplitudes used for these series of modes began at 0.5 lbf to attempt to convey the linearity of the system and then started at 1.0 lbf, increasing by an increment of 1.0 lbf to maximum forcing amplitude of 8.0 lbf. Again above this threshold the system began to oscillate and no steady state data points around resonance were captured. The resulting FRFs and transfer functions of the fourth mode of vibration as seen from the offset accelerometer may be viewed in Figure 10. Due to the similarity of the modes, the FRFs and transfer functions of the fifth mode of vibrations are not seen here but may be viewed in Appendix A.

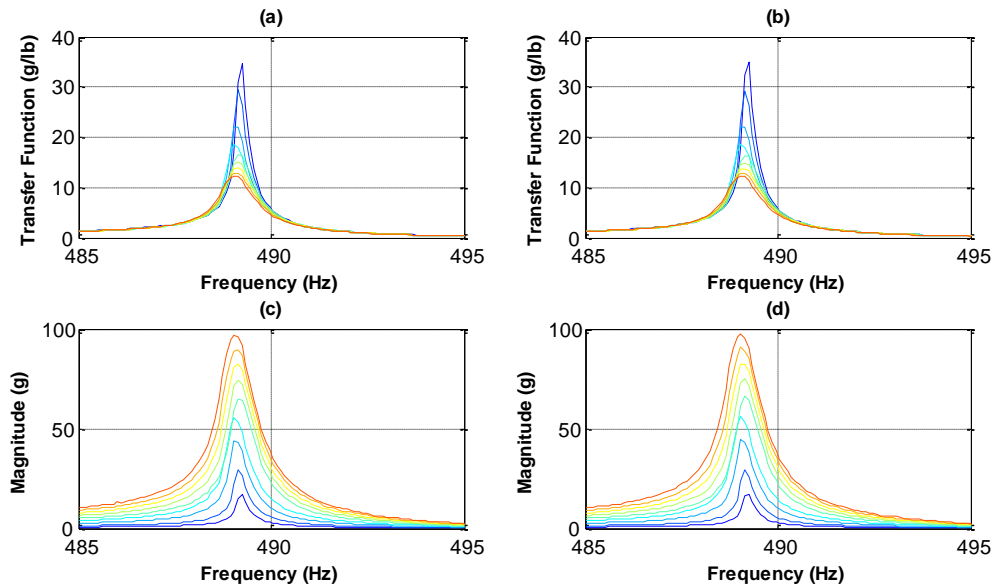


**Figure 10: Transfer function of fourth mode stepping (a) up (b) down in frequency.**

**FRFs of fourth mode stepping (c) up (d) down in frequency.**

Examining the FRFs, it can clearly be seen that the fourth mode behaves fairly linearly with only a frequency shift of 0.3 Hz. The fifth mode behaved similarly as can be seen in Appendix A. However, if one looks more closely at Figure 10(d) it can be observed that the mode initially sees a slight softening nonlinearity after which it changes to what appears to be a hardening nonlinearity. This change in nonlinearity was not observed in the first mode of vibration and yet this method of NNM extraction is still able to identify it and properly form an accurate NNM. Since the phase angle of the response passes through 90 degrees and the data points collected are close to 90 degrees, as can be seen in the phase lag plots of Figure 11 for the fourth mode and in Appendix A for the fifth mode; the phase lag quadrature criterion is fulfilled. This verifies that the NNM has



been achieved. In other words the closer the phase lag is to 90 degrees the more accurate the estimated NNM is.

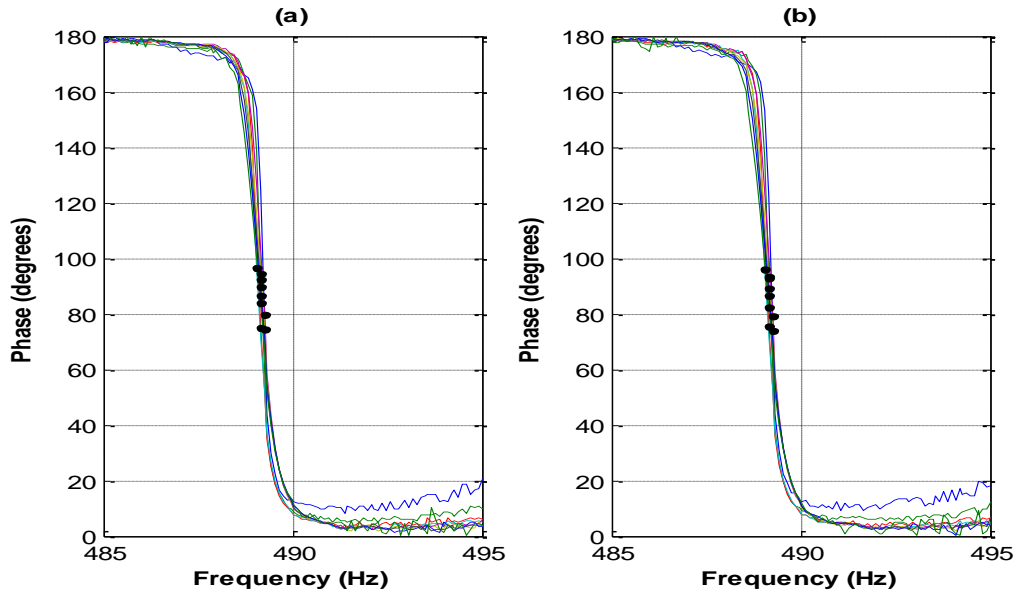


**Figure 11: Phase lag of the fourth mode stepping (a) up (b) down in frequency.**

**Markers indicate points of the fourth mode from which the NNM was extracted.**

The resulting phase lag plots of the fourth and fifth modes saw a much smoother transition from 180 degrees to 0 degrees as a result of the absence of the jump phenomena. This produces more data points along the line of interest and increases the contingent that the data points being collected occur at or near the 90 degree phase line needed to verify that the NNM has been achieved. Focusing now on the markers in Figure 11, it can be concluded that as a result of the data points mostly lying near the 90 degree phase line; that the NNM has been isolated for the fourth mode and will produce a fairly accurate NNM backbone. In contrast to the first mode of vibration and most likely

due to the linear tendencies of the mode, both the backbone curves created from stepping up and stepping down in frequency may be used to estimate the NNM.

The sixth mode of vibration behaved even more linearly than modes four and five and as a result only three forcing amplitudes were used, 0.1 lbf, 0.5 lbf and 1.0 lbf. The reason only a small maximum forcing amplitude was used was a direct result of the response amplitude becoming very high and causing the system to oscillate laterally at a lower forcing amplitude than any of the other modes. The FRFs and transfer functions examined were once again produced by accelerometer B as a result of the mode shape consisting of nodal circles and they are seen in Figure 12.

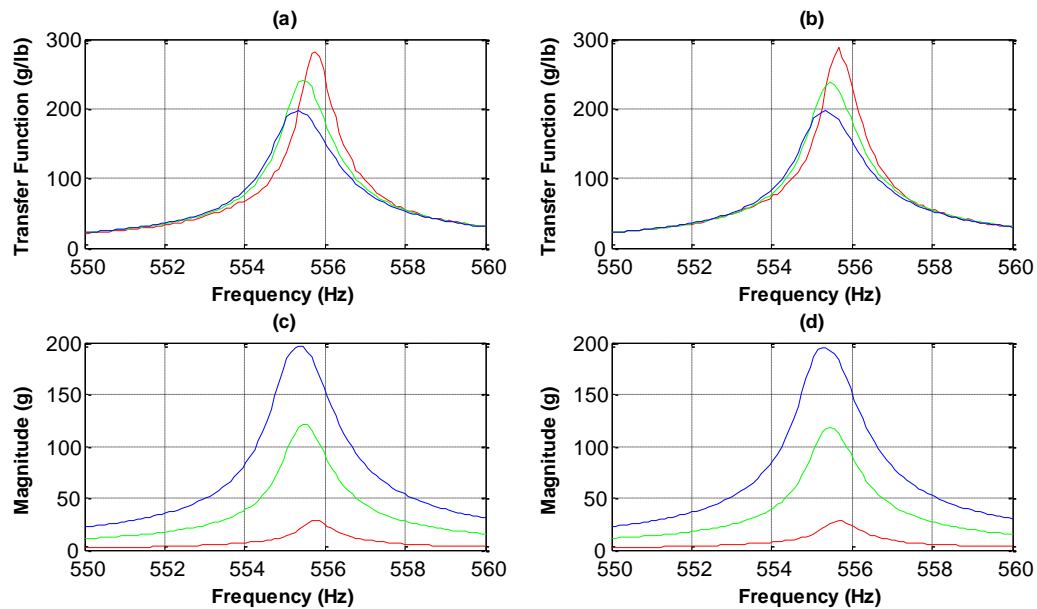


**Figure 12: Transfer function of sixth mode stepping (a) up (b) down in frequency.**

**FRFs of the sixth mode stepping (c) up (d) down in frequency.**

Only a slight frequency shift of 0.3 Hz was observed and no direct nonlinear tendencies are visible at this forcing amplitude. This produced another smooth phase lag diagram with data points at or near 90 degrees phase. The phase lag plot is seen in Figure 13 and with the phase lag quadrature criterion being confirmed for this mode, it is accepted that the NNM has been isolated, achieved and produces an accurate backbone curve when extracted.

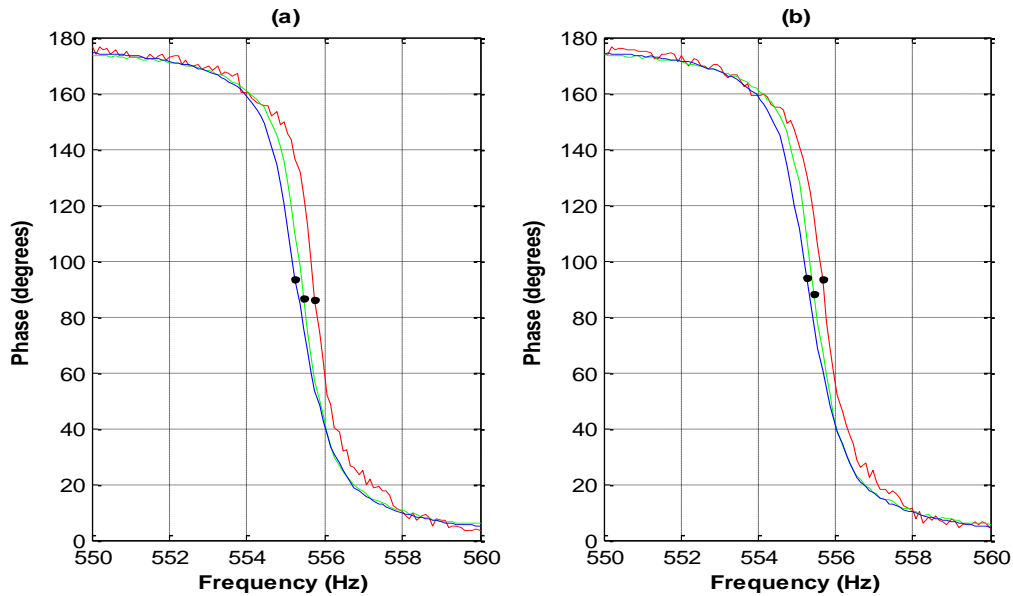


**Figure 13: Phase lag of the sixth mode stepping (a) up (b) down in frequency.**

**Markers indicate points of the sixth mode from which the NNM was extracted.**

A second plate referred to here as plate 3 was similarly tested. The only difference was that only modes one and four were investigated. Also the increment by which the forcing amplitude was increased was altered as it was thought that 30 excitation frequencies were more than enough to properly obtain the NNM. The results of the plate 3 testing may be viewed in Figures 14 through 17.

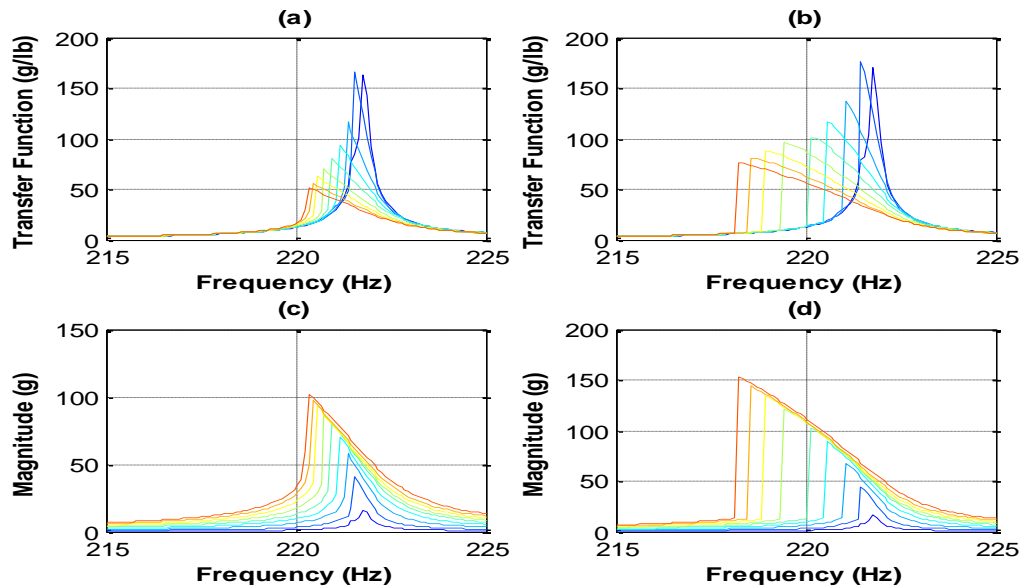


**Figure 14: Transfer function of first mode for Plate 3 stepping (a) up (b) down in frequency. FRFs of first mode for Plate 3 stepping (c) up (d) down in frequency.**

It can be seen from the FRFs, that the matching modes from both plates behave very similarly. Mode one in Figure 14 has a softening nonlinearity and mode four in Figure 16 displays a fairly linear mode with a softening nonlinearity giving way to a slight hardening nonlinearity. The phase lag diagrams also are consistent with one another confirming that the NNMs created from the FRFs would be fairly accurate; with the exception of the NNM created by stepping up in frequency of mode one. The only difference really observed between the two plates is the fact that the modes occur at different frequencies. Mode one of plate 3 occurs at roughly 15 Hz higher than mode one of the first plate. Similarly mode four occurs at a higher frequency in Plate 3.

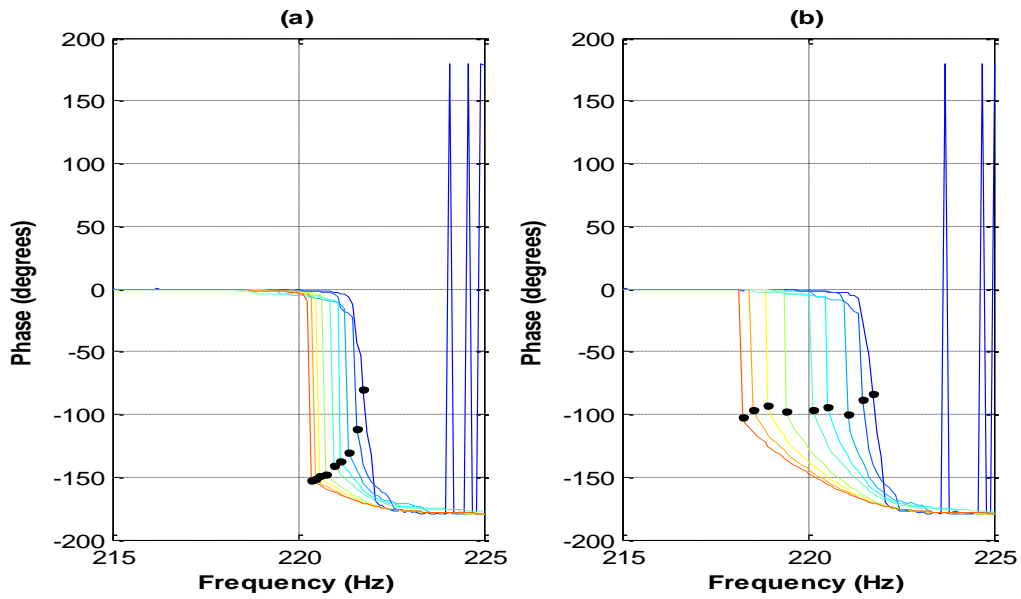


**Figure 15: Phase lag of the first mode of Plate 3 (a) stepping up. (b) stepping down in frequency. Markers indicate points of the first mode from which the NNM was extracted.**

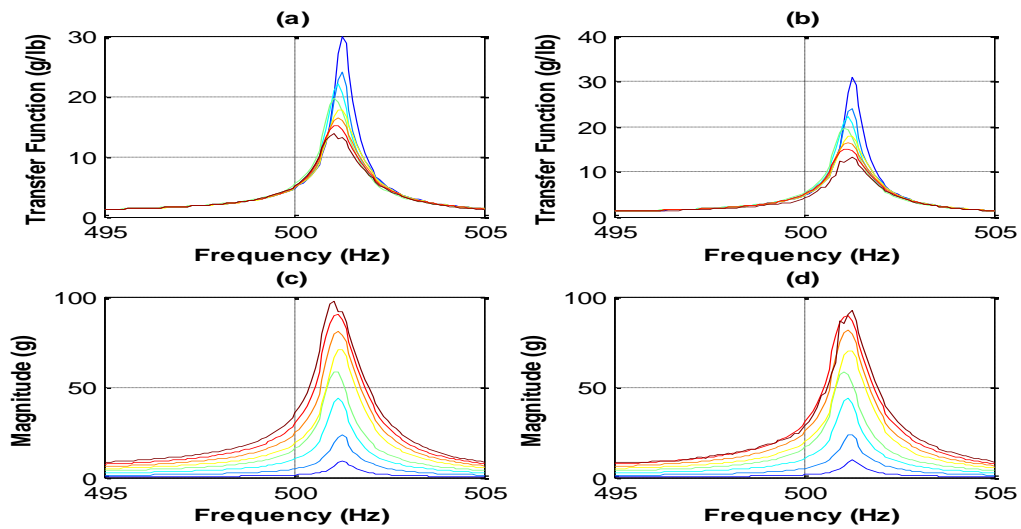


**Figure 16: Transfer function of fourth mode of Plate 3 stepping (a) up (b) down in frequency. FRFs of fourth mode of Plate 3 stepping (c) up (d) down in frequency.**

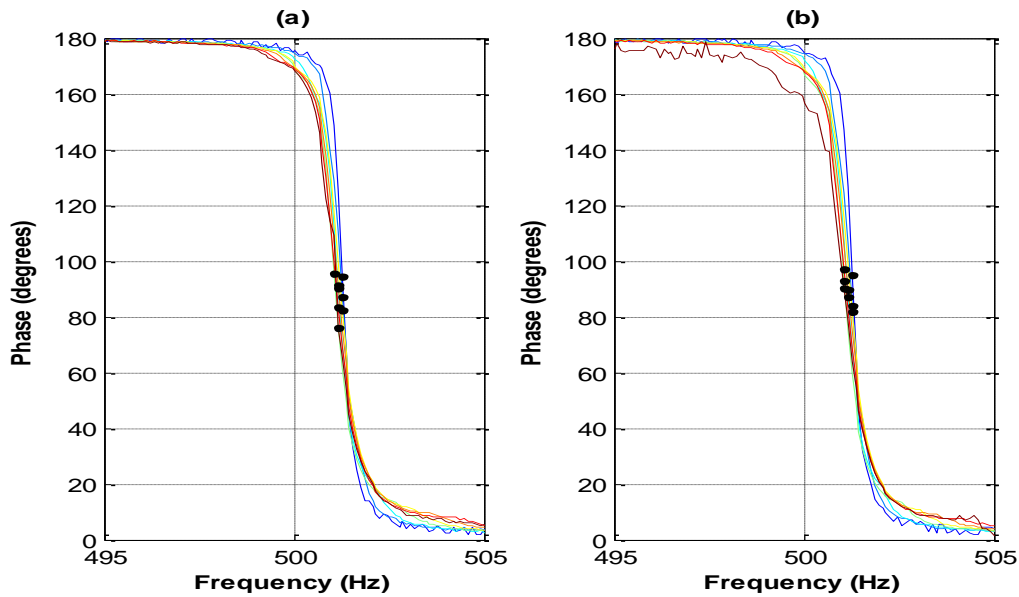


**Figure 17: Phase lag of the fourth mode of Plate 3 stepping (a) up (b) down in frequency. Markers indicate points of the fourth mode from which the NNM was extracted.**

The results from the testing of Plate 3 prove that the plates are not overly sensitive to variations that may arise from the manufacturing process. However, there is a clear difference in the natural frequencies. One theory as to why the natural frequencies are lower in the first plate is that the plate may have in-plane stresses as a result of being bent into its final shape. In plane stresses have been shown to lower the natural frequencies in structures and this change can be very significant in thin plates [22].

### 4.3 Comparison of Numerical Models to Small Shaker Tests

Once the tests had been completed, the FEM model that was generated to represent the plate's dynamics could be compared to the actual dynamics of the plate that are inherit in the estimated NNMs. Each backbone curve or approximated NNM was

extracted from the FRFs where the response occurred closest to a 90 degrees phase lag. The NNM for the first mode is shown in Figure 18 by red circles for when the program was stepping down in frequency. The green circles show the backbone curve created by the data points collected when stepping up in frequency. However, because the points are nowhere near the 90 degree phase line the curve created cannot be called a NNM. To compare, the NNM created by the original FEM model “NIC 2” is shown by the green dashed line in Figure 18.

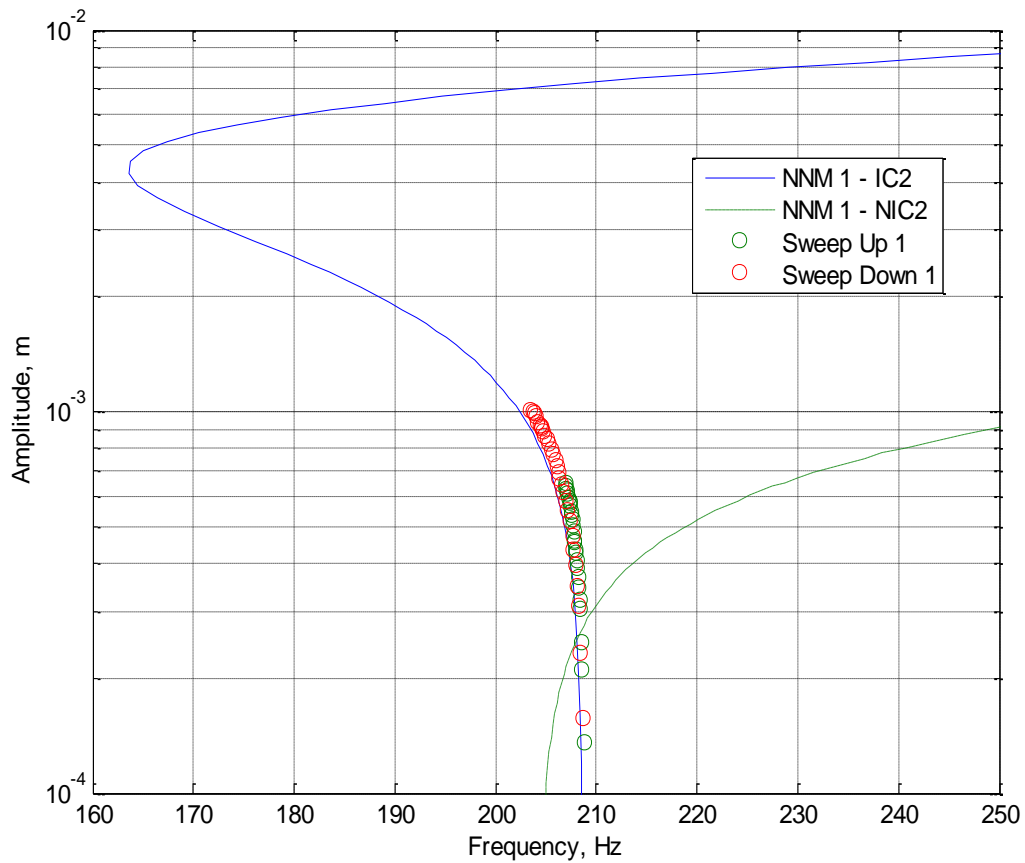


**Figure 18: Backbone comparison of the first mode of vibration**

Modes 4 and 5 are displayed in Figure 19 and mode 6 in Figure 20 with the original FEM model shown as a solid green line and the backbone curves from the increasing and decreasing frequency measurements are represented by various symbols as indicated in the figures.

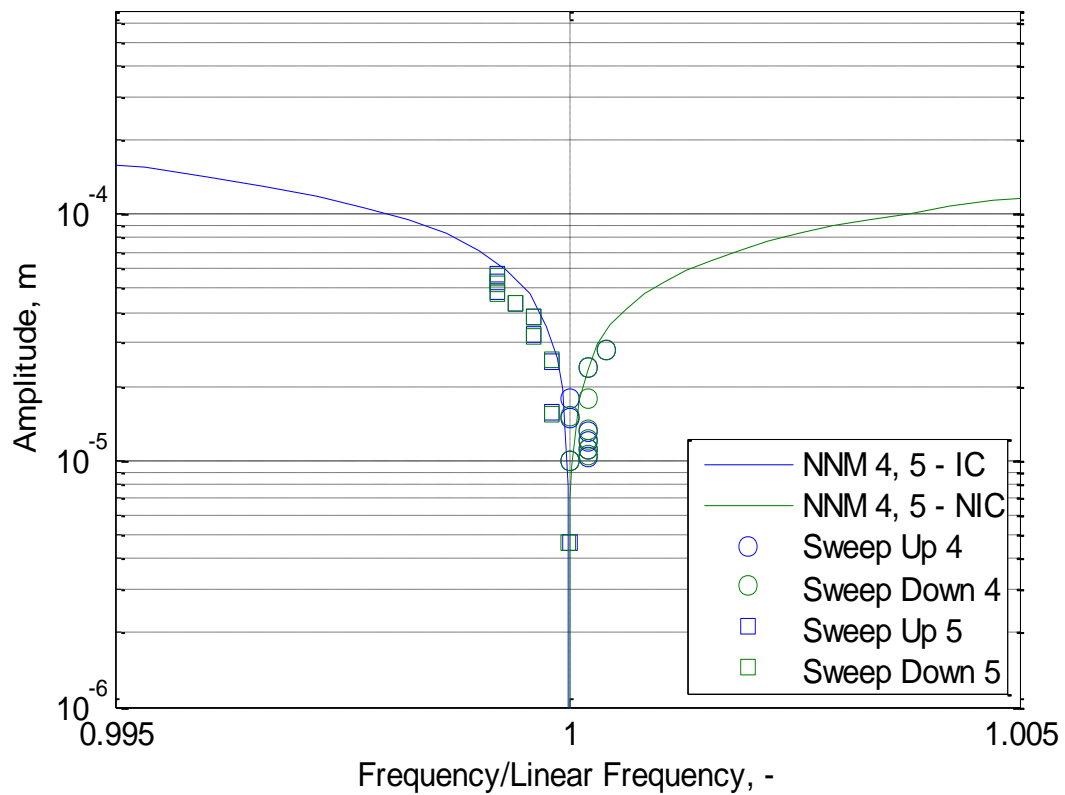


**Figure 19: Magnified view of the backbone curves of modes four and five with included linear frequency shift**



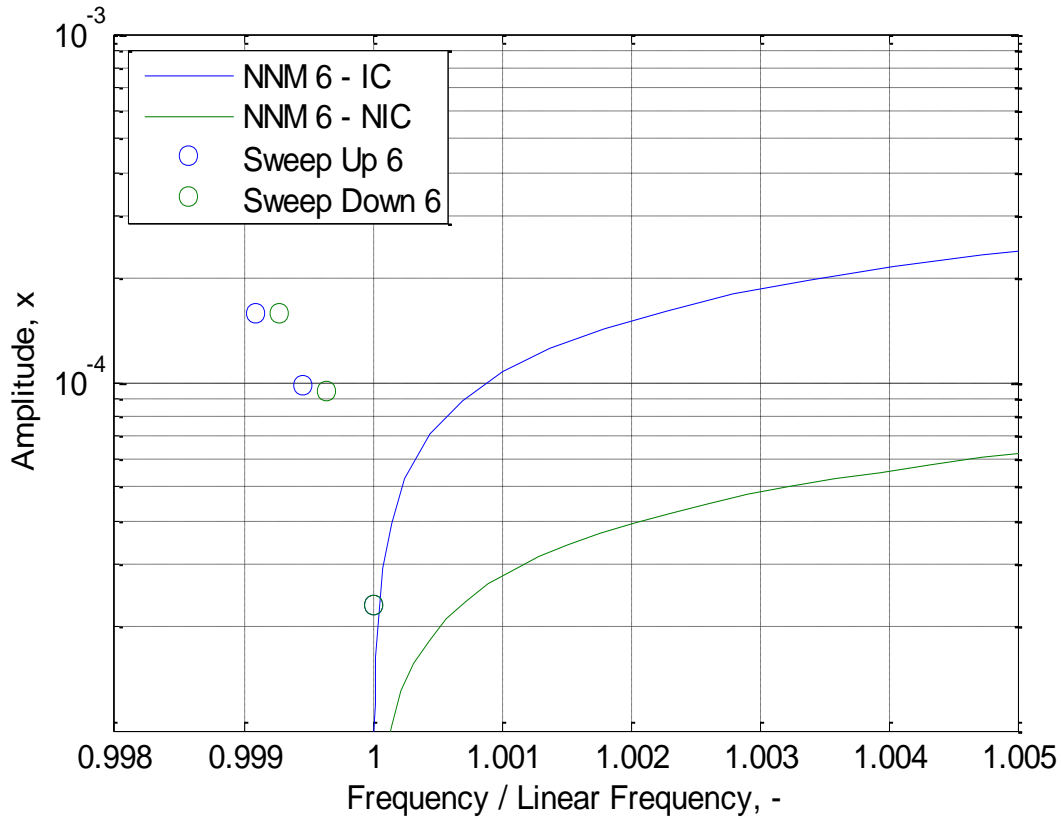


**Figure 20: Magnified view of the backbone curves of mode six with included linear frequency shift**

The energy input into the system was limited in the physical experiments by the setup but the numerical simulations were not restricted to this. Thus, the numerical simulations go out to much higher forcing amplitudes and displacements. However, even with this difference it can easily be observed that the original FEM model and the plate behave very different from one another. The FEM model's NNMs show a hardening nonlinearity for all experimented modes yet the NNMs that were extracted experimentally show a softening nonlinearity. In addition to this the FEM model doesn't properly estimate the level of nonlinearity at any given displacement. The lack of

conformity of the FEM model to the experimentally determined NNMs suggests that the assumed physics of the plate for the model were quite different in reality and required a closer look.

As was seen in the linear analysis of the plate the natural frequencies clearly have some error, but more importantly the numerically calculated NNMs exhibit very strong hardening behavior not seen in the experiments. Also, looking at the anti-symmetric modes the model reveals that they should have the same natural frequency and nonlinearity yet as seen from the experiments they exist at different frequencies and behave differently as well.

Delving into the reasons for the discrepancies seen in the model it was first determined that the geometry of the plate be once again examined; since a softening nonlinearity is an inherit property of curved plates, plates with initial compressive stress, or plates that may buckle. Looking more closely at the plate it was discovered that in actuality the plate was not flat but in fact curved out. This is most likely a result of the process used to bend the plate into its final shape. The maximum height of the plate at the center was measured as 4 mm higher than the edges of the plate. The actual topography of the plate was not surveyed however, and so it was assumed that the curvature was uniform in all directions extending out from the center and in the shape of the first linear mode. A new FEM model was created and is referred to as the IC model or plate with initial curvature.

The spring softening nonlinearity observed by the first mode of vibration was now properly modeled as can be seen in Figure 18 and the experimentally determined NNMs

agree very well with the numerically computed data. However, at larger displacements the IC model predicts the plate will experience a turning point where the softening nonlinearity will give way to a hardening nonlinearity. Modes 4 and 5 showed a softening to hardening nonlinearity even though it was subtle; yet it was not observed in the first mode at the forcing amplitudes used. Examining modes 4 and 5 in Figure 19, it can be seen that the NIC model predicts a hardening nonlinearity which the NNMs of mode 4 seem to follow, while the IC model predicts a softening nonlinearity to which mode 5 conforms. This suggests that the plate operates in a nonlinear region somewhere between both FEM models. Mode 6 is shown in Figure 20 and both IC and NIC model predict a sharp hardening nonlinearity which is not seen in the NNMs extracted experimentally.

Although the initial curvature added to the FEM seems to have corrected some of the nonlinear behavior issues, the linear natural frequencies for most of the modes are now worse than the NIC model. The comparison of the natural frequencies for the IC and NIC models before and after the elastic modulus was altered are seen from an initial hammer test in Table 6. However, unlike the previous tables in this thesis where the modes were rotated to obtain the optimum MAC values Table 6 was not rotated. Also, reviewing the MAC values from Table 6 exposes the fact that typically the mode shapes from the NIC model were more accurate than the IC model with the exception of the second, third, eighth, ninth, and fifteenth modes. In addition, there also appeared to a reordering of a few of the mode shapes in the IC model as well as a few mode shapes that did not appear at all in the experimental tests.

	$f_n$ , Test	FEM 2- NIC Mode	$f_n$ , FEM 2-NIC	%error	FEM 2- NIC MAC	FEM 2- IC Mode	$f_n$ , FEM 2-IC	%error	FEM1- IC- MAC
1	205.36	1	204.80	0.27	0.980	1	205.26	0.05	0.773
2	327.86	2	424.88	-22.83	0.686*	2	283.51	15.64	0.870*
3	348.65	3	424.88	-17.94	0.707*	3	283.51	22.98	0.835*
4	489.17	4	701.64	-30.28	0.903*	4	300.95	62.54	0.884*
5	510.22	5	702.93	-27.42	0.945*	5	303.02	68.38	0.925*
6	572.61	6	803.68	-28.75	0.945	10	578.79	-1.07	0.657
7	699.94	7	1033.70	-32.29	0.651	7	349.70	100.16	0.544
8	814.12	9	1226.10	-33.60	0.930	13	618.63	31.60	0.736
9	827.68	10	1226.10	-32.50	0.906	14	618.63	33.79	0.750
10	916.77	11	1421.70	-35.51	0.933	8	465.22	97.06	0.934
13	938.96	12	1424.00	-34.82	0.941	9	466.01	101.49	0.941
14	1096.27	13	1713.70	-45.21	0.956	15	688.16	59.30	0.938
15	1178.72	15	1817.40	-35.14	0.444				
16	1191.36	16	1872.10	-36.36	0.401	12	615.51	50.79	0.488
17	1200.57	17	1872.10	-35.87	0.431	11	615.51	48.96	0.623

**Table 6: Comparison of the linear natural frequencies with curvature of the model excluded (FEM 2-NIC) and included (FEM 2-IC)**

The above discrepancies have not yet been investigated, yet it is hypothesized that again the curvature of the plate may in fact still remain the main culprit for the deviations. As previously stated, the complete topography of the plate was not surveyed and therefore it is a possibility that the plate does not slope uniformly from the edges to the center and may consist of peaks and valleys. The actual measurement technique used to measure the center height was not conventional because the plate did not sit flat within the cylinder it was welded into. To estimate the height of the center of the plate four points along the outer diameter of the can were measured and compared to the center height of the plate culminating in 4 different height measurements of 3.31 mm, 3.7 mm,

5.01 mm, and 5.03 mm. Thus, it can be seen that the assumption that the center of the plate was elevated 4 mm from the edge of the plate to the center was incorrect and further investigation into this aspect of the plate's geometry is required. Another probable cause of the deviations in natural frequency and mode shapes could be from the fact that the forming process of the exhaust plate assembly may cause internal residual stress' which will in fact change the dynamics of the plate and are not properly modeled in either the NIC or the IC FEM. A third possibility for disparity in the FEM models and the experimental results may be from the assumption that the plate is isotropic. The procedure that was used to model the effective elastic modulus in [16] makes such an assumption. However, the hole pattern of the perforations should make the plate orthotropic and the direction of the nodal diameters reveals where the plate is actually stiffer. Finally, the assumption that the plate was axisymmetric was proven to be false as the anti-symmetric modes appeared at different frequencies in the experimental testing while they had the same natural frequency in both the FEM models. All of these listed theories explaining as to why the model with initial curvature did not match more closely with the experimental data will require further attention to properly model the structure. To continue this study, the next step would be to investigate the linear and nonlinear comparisons as to why they don't match and adjust the parameters within reason until they match. This may prove difficult though as the NNMs appear to be sensitive to geometry, residual stress and possibly other unaddressed parameters.

## 5. Experimental Setup for Large Shaker Tests

Examining the nonlinear dynamics revealed in the FEM model with initial curvature, specifically the first mode of vibration; reveals a softening nonlinearity that deviates at higher excitation energy towards the hardening nonlinearity. In Figure 18, it can be seen that the NNM matches closely with the numerical simulation as they both soften but the physical experiments were not carried out with a strong enough forcing amplitude to observe whether or not the NNM would ever reach the turning point in the numerical simulation and change from a softening to hardening nonlinearity. To better verify the model and witness the possible turning point of the NNM, another set of stepped sine measurements were taken; except they were performed on a much larger shaker and without a stinger. This was done in order to negate the oscillations of the system that limited the magnitude of the forcing amplitudes.

The larger forcing amplitudes for the stepped sine measurements were provided by a Ling Dynamics V830-335 SPA10K (RM) electrodynamic shaker capable of a 9807 Newtons (2205 lbf) sine forcing amplitude. Instead of driving the plate with a stinger, the larger shaker allowed for the base plate of the plate assembly to be bolted directly to it as seen in Figure 21. With no stinger to excite the plate assembly the force transducer was removed from the setup and the quasi-closed loop control function of the SignalCalc software was now controlled by a 25 g K-Shear accelerometer with a sensitivity of 200 mV/g. This accelerometer was mounted to the base plate via wax as seen in Figure 21. The plate was bolted to the base plate in the same manner that it was for the smaller shaker tests and the two ISOTRON 25B accelerometers with nominal sensitivities of 5 mV/g that were used in the small shaker tests were again used for the large shaker tests

(See Table 5). These accelerometers were again placed in the center of the plate to identify modes with nodal circles and at one third the radius from the center of the plate to identify the modes with nodal diameters. All accelerometers were secured using wax even though the forcing amplitudes that were experienced were much higher than previous tests. The ABACUS data acquisition hardware and SignalCalc software were used for the tests with larger forcing amplitudes. The experimental setup may be viewed in Figure 22.

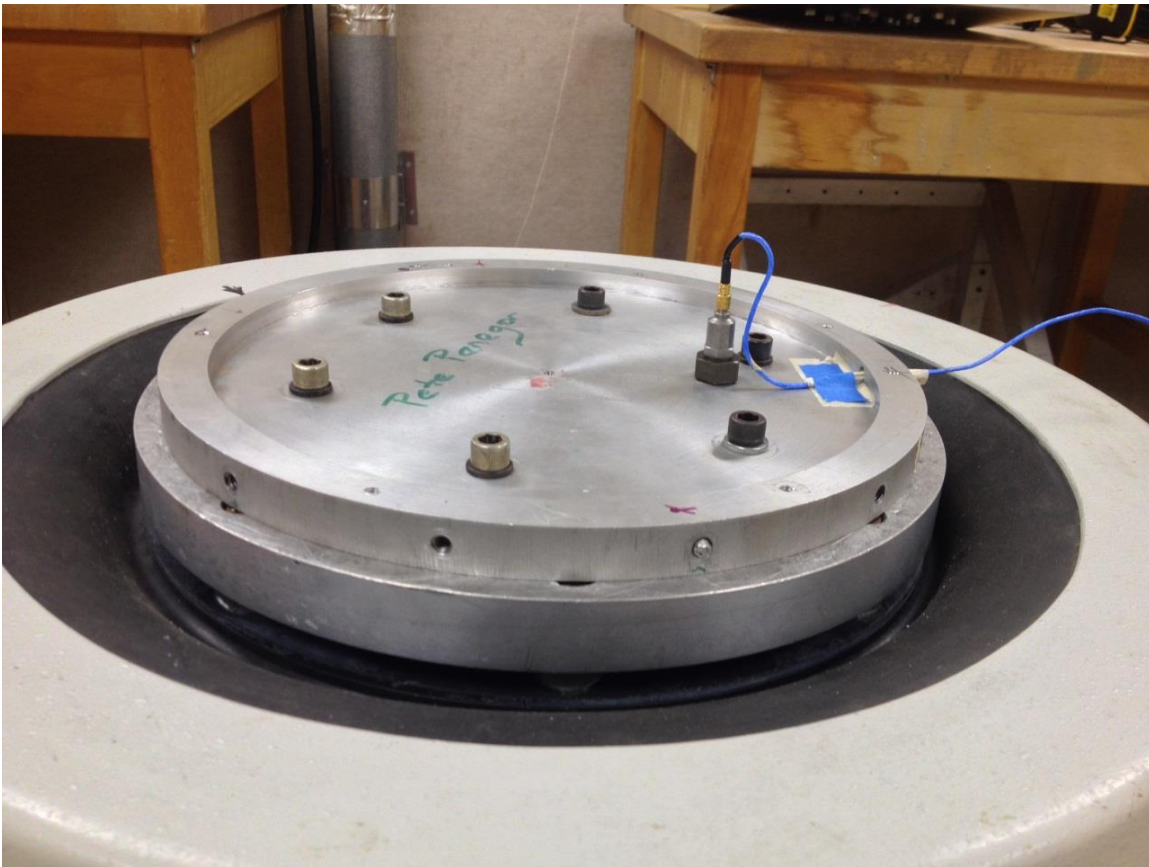


**Figure 21: Base plate attached to fixture plate on large Ling Dynamics modal shaker**



**Figure 22: Experimental Setup with Ling Dynamics V830-335 SPA10K (RM) modal shaker and ABACUS data acquisition hardware**

With the absence of the force transducer to set the forcing amplitude directly in the software it had to be converted into g's from Equation 15.

$$a_{cel} = \frac{F_a}{Mg} \quad (15)$$

where  $a_{cel}$  is the acceleration in g's of the base plate,  $F_a$  is the desired forcing amplitude,  $M$  is the total mass of the system; which includes the mass of the base plate, the mass of



the armature, the mass of the fixture plate, the mass of the test plate, and the mass of the mounting bolts and washers, and  $g$  is the acceleration due to gravity.

Initially, it was attempted to try to begin the larger shaker tests at the highest forcing amplitudes from the smaller shaker tests but because of the added weight of system, the accelerometer would not control properly at such low accelerations and would never reach a steady state or would never accurately control at the prescribed acceleration. As a result, all of the tests on the large shaker began at 100 lbf forcing amplitudes and were increased by an increment of 25 lbf to various maximum forcing amplitudes based on the response of the system.

Compared to the small shaker, the large shaker was able to reach steady state at each step quicker than the smaller shaker and therefore, a larger bandwidth was selected to allow the system to start from a low response and then after resonance attempt to return to a low response. Each test had a bandwidth of 50 Hz and yet still only 100 data points were taken for each test to attempt to extract the NNMs from the FRFs.

### **5.1 First mode of Vibration on Large Shaker**

The first mode of vibration occurred at around 205 Hz and therefore a bandwidth of 50 Hz ranging from 170 Hz to 220 Hz was chosen. Using the quasi-closed loop algorithm in the shaker control software, the acceleration stayed within 10% of the target value. The bandwidth was stepped through using 100 data points both increasing and decreasing in frequency. Figure 23 displays the results of the stepped sine measurements as recorded by the center accelerometer starting from forcing amplitude of 100 lbf and increasing by an increment of 25 lbf until maximum forcing amplitude of 425 lbf was achieved. A

stepped-sine measurement was attempted at 450 lbf but at this forcing amplitude the system began to demonstrate what appeared to be chaotic behavior and the system never reached steady state around resonance. Observing the FRFs in Figure 23 and Figure 24, it can clearly be seen that the overall shape of the FRFs recorded by accelerometer B and accelerometer C are different. At the lower forcing amplitudes the softening nonlinearity seen in the smaller shaker tests is evident. However, at higher forcing amplitudes the two FRFs begin to display different responses. Accelerometer B in the center of the plate begins to have an intermediate step in the jump phenomena that is seen at lower forcing amplitudes. As a result of only having the FRFs and NNMs, it is unclear as to what is causing the intermediate amplitude. Further investigation would have to be conducted in order to narrow down what is causing the change in behavior. While accelerometer C does not see the intermediate step that accelerometer B does, there is a change in the behavior of its jump phenomena as well. At lower forcing amplitudes the jump occurs at the peak of the response as it did in the small shaker tests. However, at higher forcing amplitudes the response begins to decay slowly at first and then the jump phenomena suddenly develops.

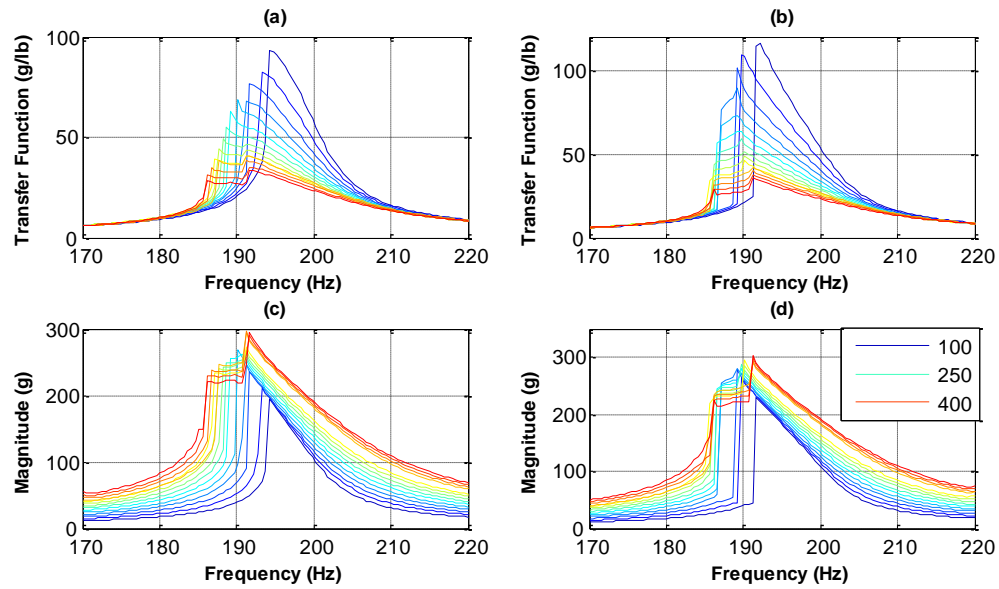


**Figure 23: Accelerometer B. Transfer functions of first mode stepping (a) up (b) down in frequency. FRFs of first mode stepping (c) up (d) down in frequency**

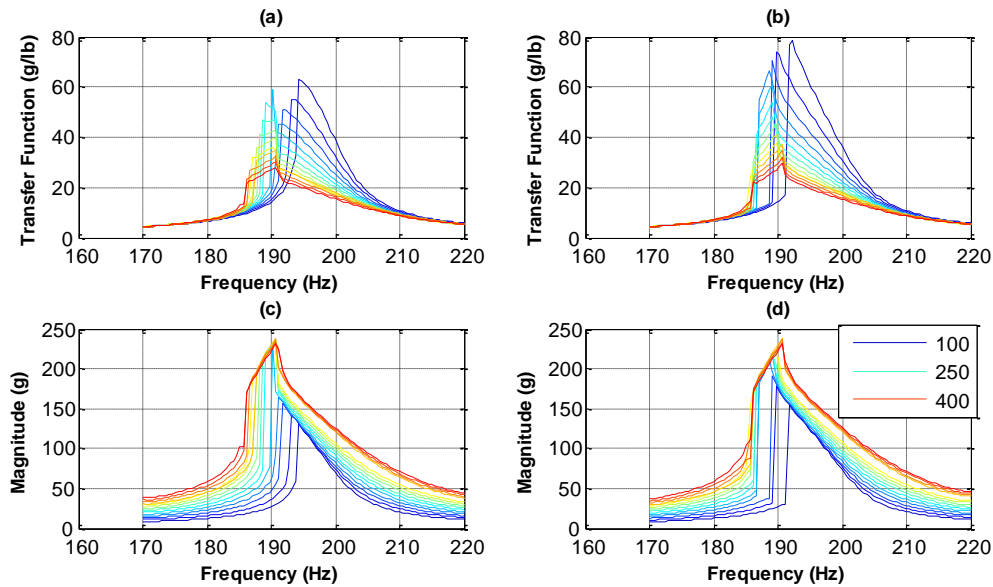


**Figure 24: Accelerometer C. Transfer functions of first mode stepping (a) up (b) down in frequency. FRFs of first mode stepping (c) up (d) stepping down in frequency**

One conclusion that may be drawn from the difference in the behavior seen in the two accelerometers FRFs is that they no longer show that there is one mode shape active at this frequency. The first mode, as seen in Table 1; consists of one nodal circle created by the boundary. Regardless of the amplitude applied to the system, if only mode one is active then the ratio of the response between the two accelerometers should stay constant. However, at higher forcing amplitudes this ratio between the two accelerometers changes and they no longer display what looks like one constant mode shape. To investigate this change in behavior the first six harmonics were recorded and reviewed. While all the harmonics displayed some response around resonance; the second and fifth harmonic displayed a much higher response and can be seen in Figures 25 and 26 respectively.

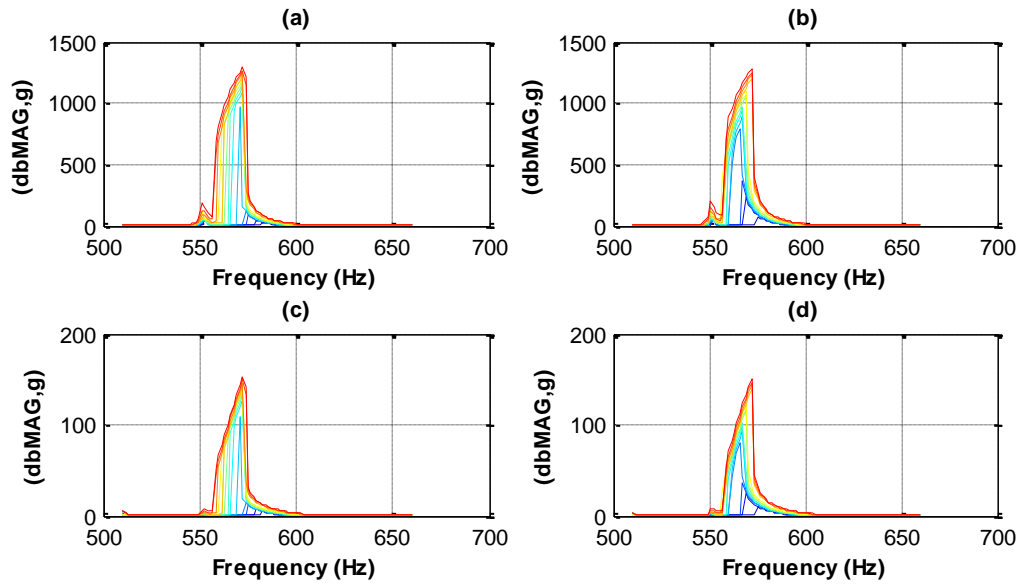


**Figure 25: Second harmonic observed from accelerometer B stepping (a) up (b) down in frequency. Second harmonic observed from accelerometer C stepping (c) up (d) down in frequency**

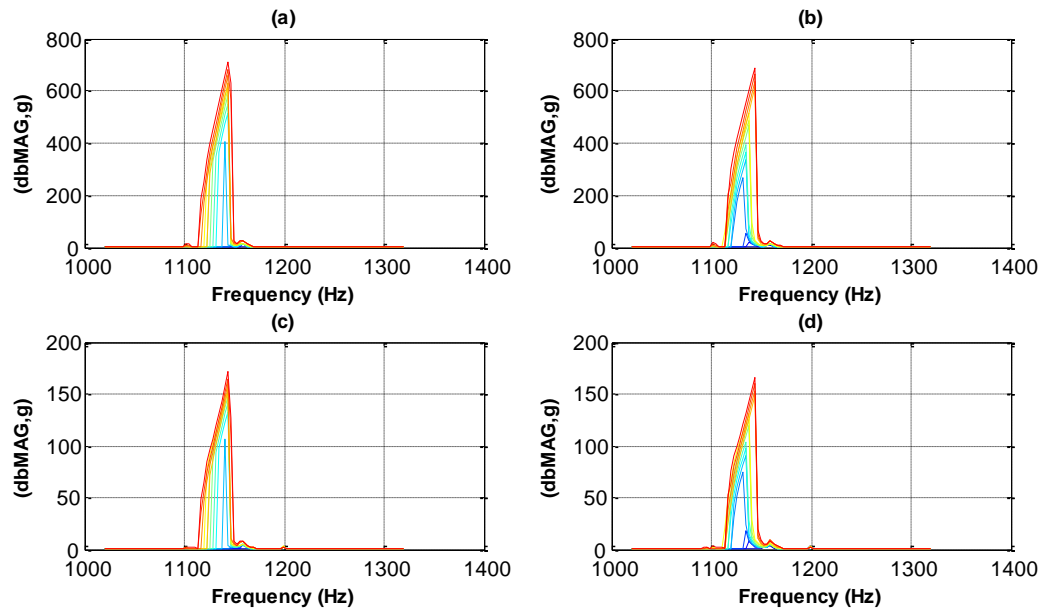


**Figure 26: Fifth harmonic observed from accelerometer B stepping (a) up (b) down in frequency. Fifth harmonic observed from accelerometer C stepping (c) up (d) down in frequency**

Accelerometer B experiences the highest response from the second harmonic which occurs in the neighborhood of the sixth mode. From the hammer tests it was observed that the sixth mode shape consisted of two nodal circles. Therefore, it is a possibility that due to the high response seen in the second harmonic that the sixth mode shape is being seen as well. Using a strobe light and adjusting it manually as the frequency changed, a definite shift in mode shapes was observed. It is thought that this other mode shape consisted of two nodal circles but it was not definitive.

Accelerometer B experiences another high response from the fifth harmonic. The mode shape at this frequency was not investigated as the second harmonic would

dominate. However, there is most likely some contribution from this harmonic to the overall response of the first mode at higher forcing amplitudes. Further investigation into the harmonics would be required to understand their combined contribution.

Further examining the FRF behavior in Figure 23, it is thought that what is being seen is the softening nonlinearity shifting to that of a hardening nonlinearity, as seen in the FEM model with initial curvature. However, it still seems unclear whether or not this dynamic behavior is actually occurring. Therefore accelerometer C, which would not see as high a response or be subject to the displacements of accelerometer B, was examined and the results can be seen in Figure 24. Accelerometer C produces a much smoother set of FRFs over the same bandwidth and from these plots a stiffening of the plate looks like it may be occurring but it is still very unclear if the hardening nonlinearity is beginning to appear.

To verify that the data points collected create accurate NNMs, the phase lag quadrature criterion must be checked once again. The resulting phase lag diagrams of the stepped sine measurements can be found in Figure 27 for accelerometer B and Figure 28 for accelerometer C. Examining the phase diagram from accelerometer B first, it can be seen that when the program was stepping up in frequency that the points closest to 90 degrees are pretty spread out. Therefore, creating a backbone curve from the points collected would not produce that accurate of an NNM. When the program is stepping down most of the data points occur below 90 degrees with a decent amount of error. Thus, again the NNM created from these points would not be that accurate.

Analyzing the phase lag diagram in Figure 28 it can be seen that the overall shape of the diagram is similar to the diagram generated by the phase lag from accelerometer B. Therefore, using either data sets from accelerometer B or C would not give a fairly accurate NNM for the first mode of vibration. The reasons as to why the system was unable to properly capture data points near the 90 degree phase are unknown. It could be due to the fact that the plate begins to stiffen and the jump phenomenon has an intermediate step. Whatever the reason, the first mode of vibration was characterized more accurately in the NNM created by the small shaker in Figures 8 and 9.

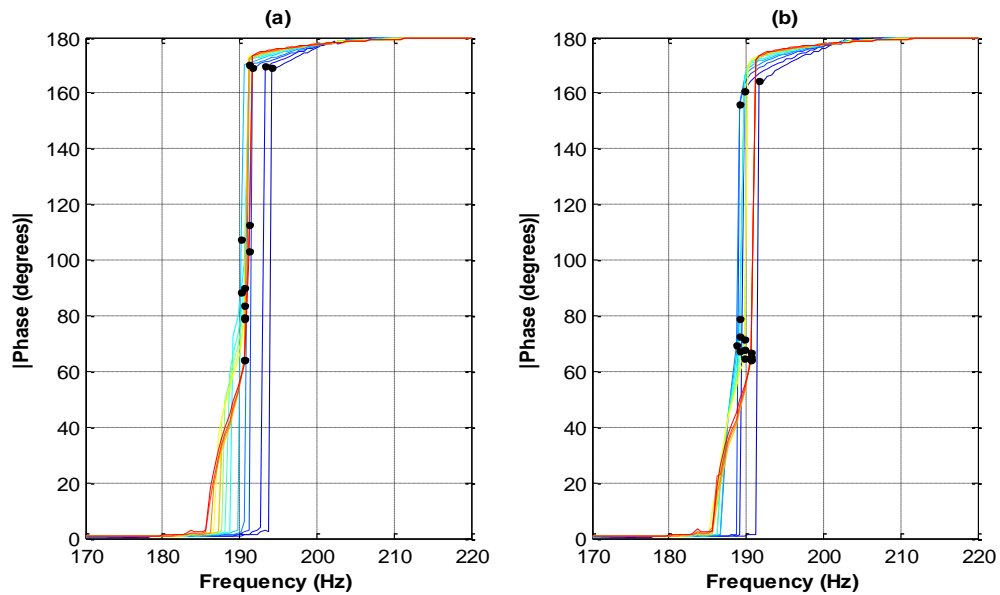


**Figure 27: Accelerometer B. Phase lag of the first mode stepping (a) up (b) down in frequency. Markers indicate points of the FRF of the first mode from which the NNM was extracted**



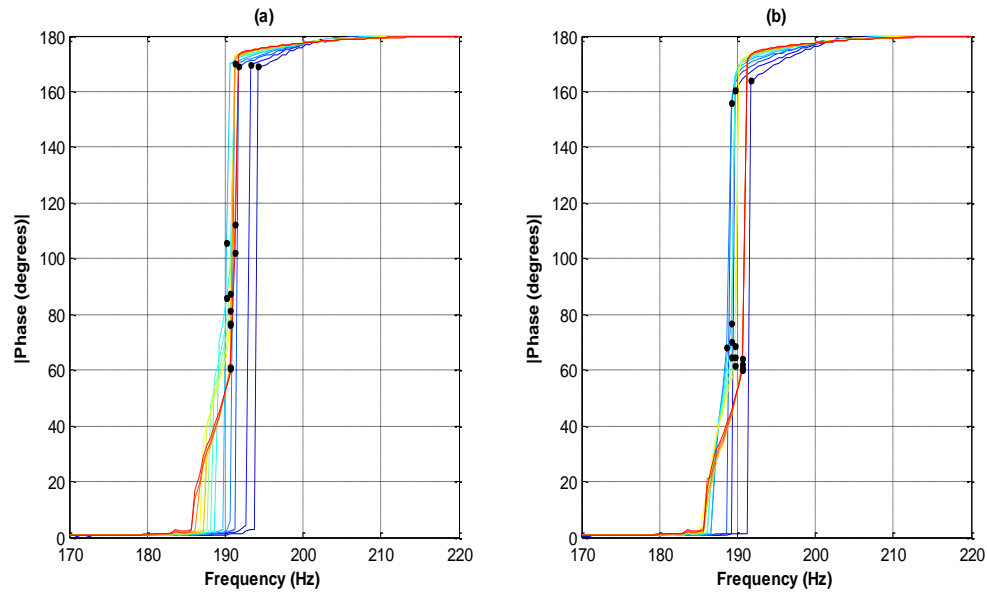


**Figure 28: Accelerometer C. Phase lag of the first mode stepping (a) up (b) down in frequency. Markers indicate points of the FRF of the first mode from which the NNM was extracted**

## 5.2 Second and Third Modes of Vibration on Large Shaker

The small shaker tests for the second and third modes behaved fairly linearly and as a result the larger shaker tests were examined to see if the modes exhibited any nonlinear softening or hardening effects at higher forcing amplitudes. Figures 29 and 30 shows the respective responses of accelerometers B and C to a range of forcing amplitudes starting with 100 lbf and increasing by an increment of 25 lbf until maximum of 450 lbf was achieved. Even at these high forcing amplitudes the system again behaves fairly linearly and quite possibly requires more excitation energy to drive it into a nonlinear range. It is interesting to note that these two modes should be modes consisting of nodal diameters and yet the center accelerometer experiences a higher response than the offset

accelerometer at the second mode. It is a possibility that for the second mode, accelerometer C rested very near one of the nodal diameters while for the third mode the nodal diameter rotated allowing for the accelerometer to once again measure a response at that point. Another possibility is that a zero exists between the two modes.

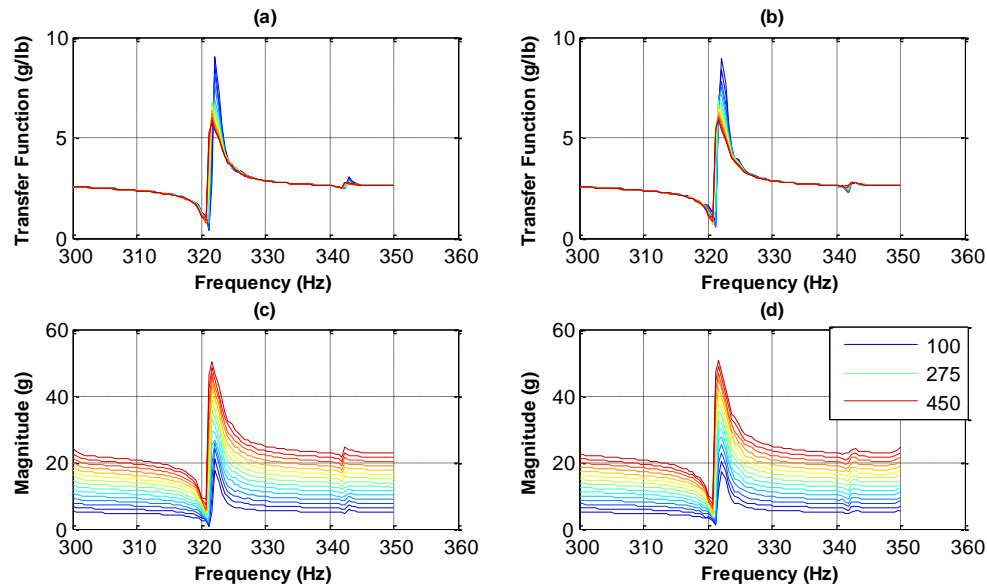


**Figure 29: Accelerometer B. Transfer functions of second mode stepping (a) up (b) down in frequency. FRFs of second mode stepping (c) up (d) down in frequency**

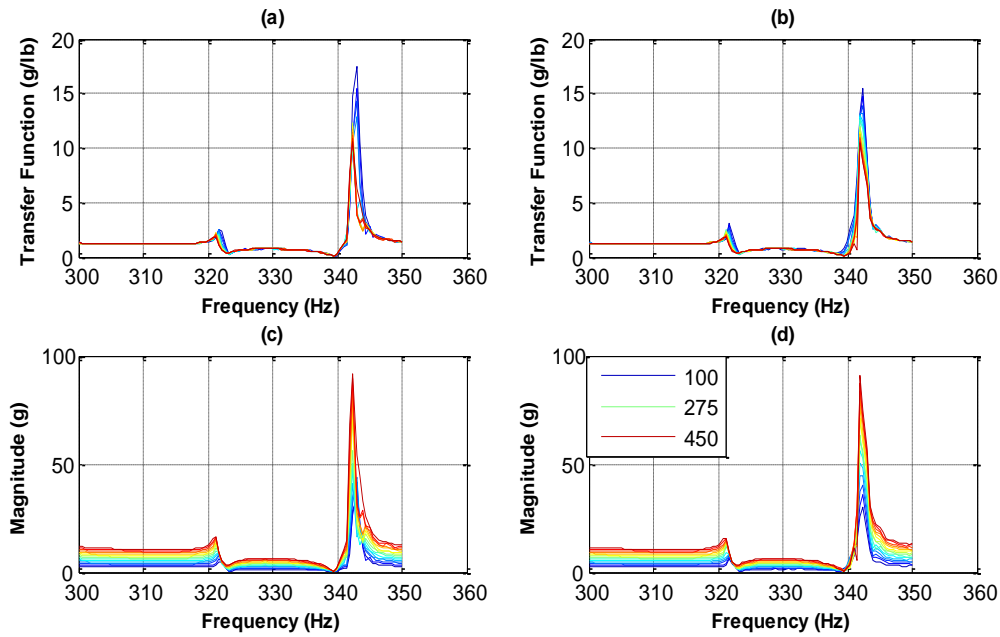


**Figure 30: Accelerometer C. Transfer functions of third mode stepping (a) up (b) down in frequency. FRFs of third mode stepping (c) up (d) down in frequency**

The phase lag diagrams of the second and third mode are shown in Figures 31 and 32, and because the points shifted between -180 degrees and 180 degrees so much over the course of the experiment the absolute value of the plots was taken to make it more legible. Again the program seems to have the same problems observed in the first mode of vibration. The data points selected occur on a 40 degree range for accelerometer B. Giving what would be an inaccurate NNM. Similarly, the data points in Figure 32 are spread at a decent interval. This would produce another NNM that would be inaccurate. Interestingly, we observe the same problem in modes 2 and 3 that we see in mode 1, with no large number of data points at the 90 degrees turning phase point. However, in modes 2 and 3 there is an absence of apparent nonlinearity. Therefore, it can be concluded that

the reason the program is unable to capture a point at the 90 degrees phase point is not due to the nonlinearity and thus exposing a weakness of using the larger shaker.

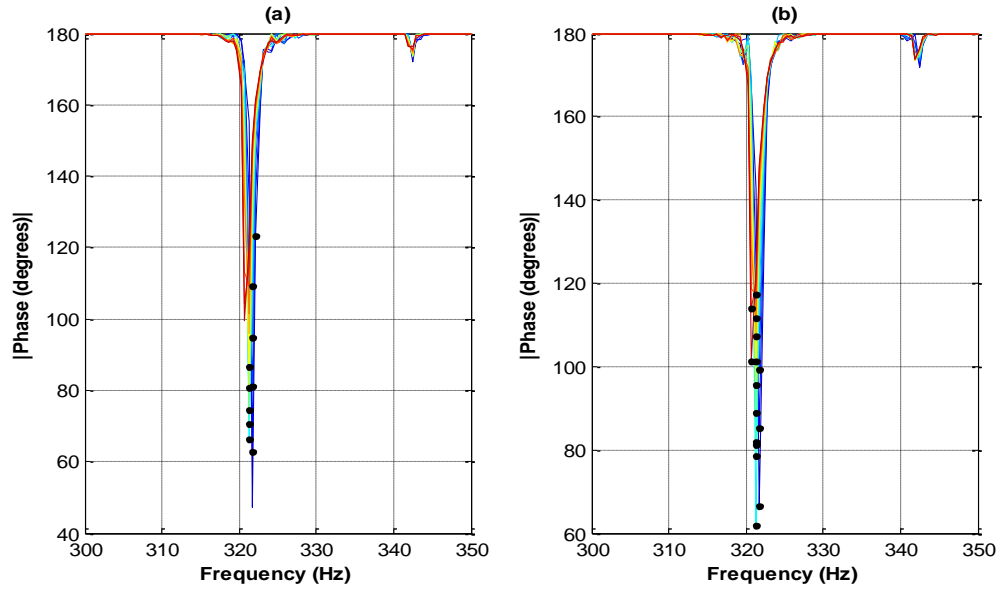


**Figure 31: Accelerometer B. Phase lag of the second mode stepping (a) up (b) down in frequency. Markers indicate points the FRF of the second mode from which the NNM was extracted**

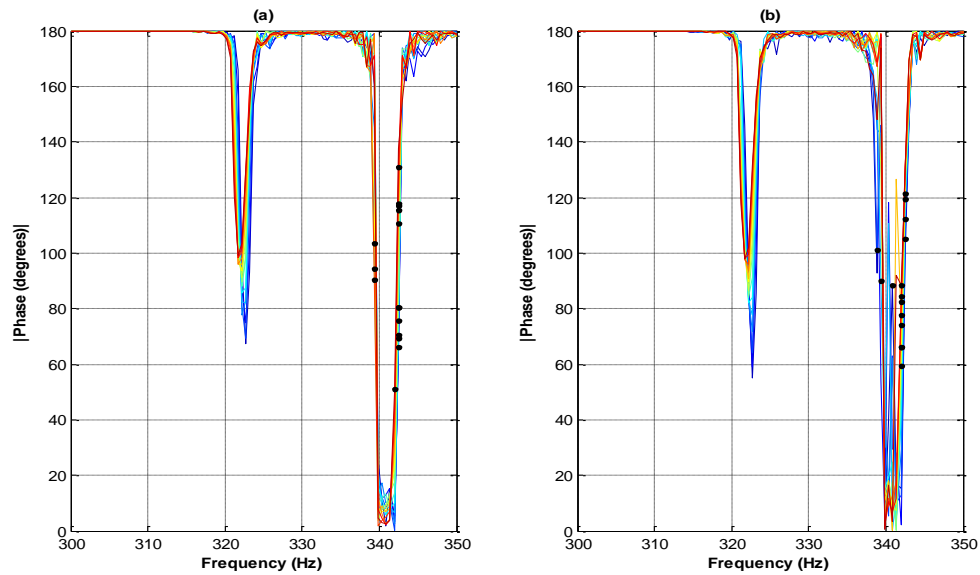


**Figure 32: Accelerometer C. Phase lag of the second and third mode stepping (a) up (b) down in frequency. Markers indicate points of the FRF of the third mode from which the NNM was extracted**

### 5.3 Fifth and Sixth Modes of Vibration on Large Shaker

Similar to how the second and third modes were examined; the fifth and sixth modes of vibration were looked at together even though their mode shapes were not the same. The fifth mode exhibits behavior common with modes with two nodal diameters while the sixth mode behaves like a mode with two nodal circles. Much like the sixth mode on the small shaker the sixth mode again saw very high responses to the excitation energy placed into the system, limiting the forcing amplitude to a maximum of only 150 lbf. At this forcing amplitude, the response of the accelerometers was over 800 g's and they would have overloaded at 1000 g's. Therefore, only 3 stepped sine measurements were taken starting at 100 lbf and increasing by 25 lbf. The results of the stepped-sine

measurements are seen in Figures 33 and 34. The FRF of accelerometer B sees the highest response in the sixth mode while accelerometer C experiences the highest response for the fifth mode. Figure 33 is a zoomed in display of simply mode six, as mode five was dormant at accelerometer B. At such high excitation energy a clear hardening nonlinearity begins to form. This is in agreement with the hardening nonlinear behavior that was predicted for the sixth mode in the FEM model seen in Figure 20.

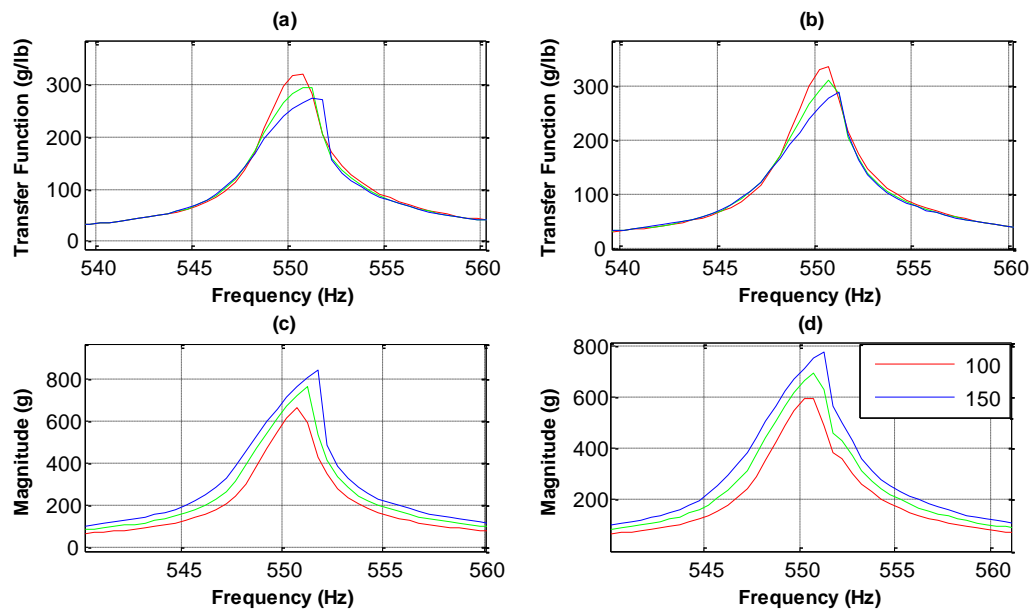


**Figure 33: Accelerometer B. Transfer functions of sixth mode stepping (a) up (b) down in frequency. FRFs of sixth mode stepping (c) up (d) stepping down in frequency**

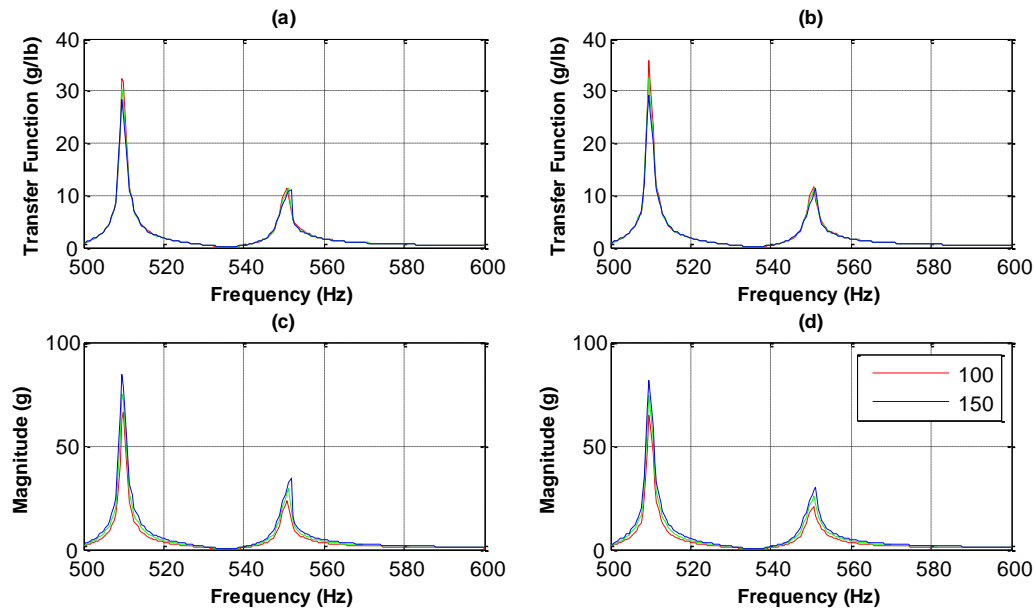


**Figure 34: Accelerometer C. Transfer functions of fifth and sixth modes stepping (a) up (b) down in frequency. FRFs of fifth and sixth modes stepping (c) up (d) down in frequency**

The phase lag diagrams of the fifth and sixth modes are seen in Figures 35 and 36 respectively. Figure 35 displays the points collected near 90 degrees of the fifth mode and unlike the previous shaker tests they are very close to the 90 degree phase line required to fulfill the phase lag quadrature criterion. Similar to Figure 35, Figure 36 shows that the collected points of the sixth mode when stepping down in frequency as captured by accelerometer C is near a phase of 90 degrees. With both modes acquiring data points near 90 degrees the NNMs extracted from the FRFs will be a good estimation of the actual NNMs. The high accuracy is probably due to the mostly linear behavior of the modes. This result was also seen on the smaller shaker and the only extra data that

was obtained by using the larger shaker was that the mode 6 showed a stronger stiffening effect.

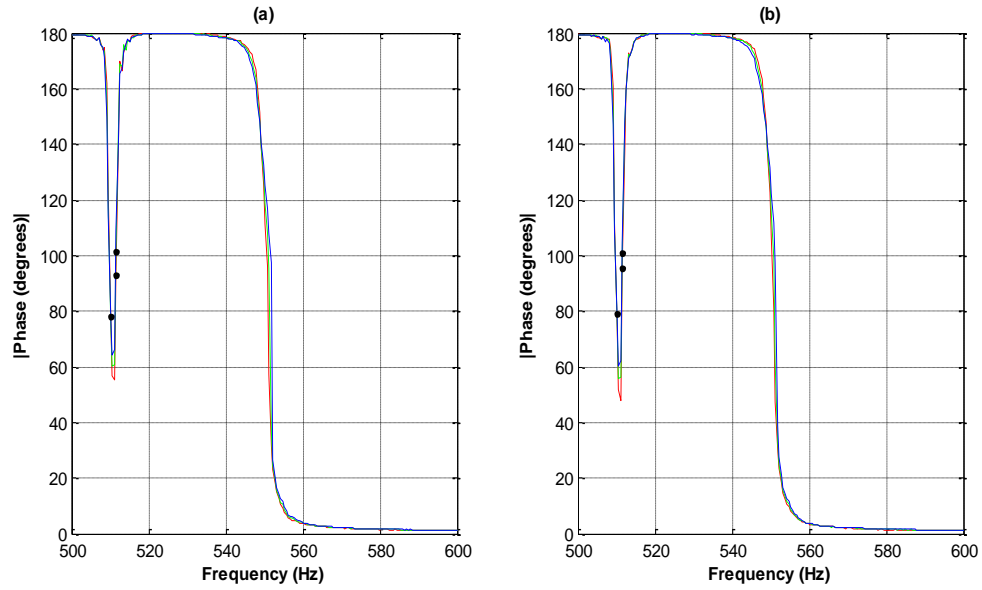


**Figure 35: Accelerometer B. Phase lag of the fifth and sixth mode stepping (a) up (b) stepping down in frequency. Markers indicate points of the FRFs of the fifth mode from which the NNM was extracted.**



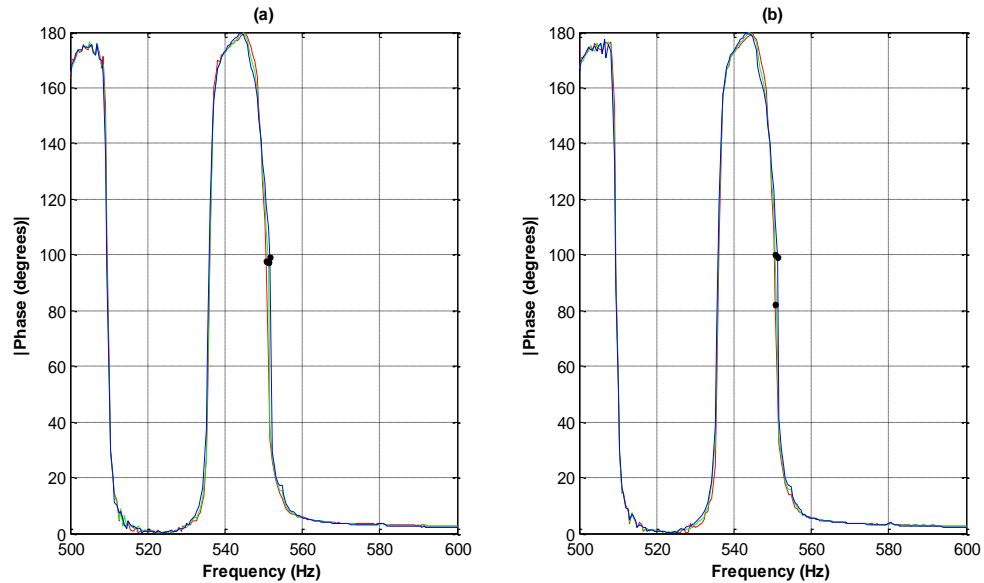


**Figure 36: Accelerometer C. Phase lag of the fifth and sixth modes stepping (a) up (b) down in frequency. Markers indicate points of the FRFs of the sixth mode from which the NNM was extracted.**

#### 5.4 Comparison of Small Shaker to Large Shaker NNMs

While the larger shaker was able to allow the system to bypass the laterally oscillating behavior that occurred in the small shaker tests and therefore allow for higher forcing amplitudes; it did not however improve the results. Simply looking at the phase plots created by the first modes of vibration when stepping down in Figure 9 for the small shaker test and Figures 27 and 28 for the large shaker tests, it can clearly be seen that the NNMs created on the smaller shaker would be more accurate. This is consistent with the other modes investigated on the larger shaker. The only time where the NNMs of the larger shaker produce the same or more accurate results occur when the modes are

consistently more linear. This however is not a true benefit as the whole point of the process is to extract NNMs from nonlinear systems.

The larger shaker did however help to show that the stiffening effect seen in the FEA model seems to be occurring, verifying that at least the FEA model is possibly correct in modeling that behavior. On the other hand, the jump phenomenon has an intermediate step in the larger shaker tests for the first mode of vibration and it is unclear as to why this occurs. Therefore, the larger shaker tests produced more questions than answers when compared to the tests performed on the small shaker. Of course, this is strictly a result of the system being tested and nonlinear behavior of other systems will vary. Thus, it is recommended that for this method a small shaker will more accurately produce NNMs than a larger shaker.

## **6. Conclusion**

In this thesis, a method to experimentally extract and validate the nonlinear normal modes of a circular perforated plate was investigated. This was performed by using a modal shaker to apply a stepped-sine excitation to the structure at individual modes of vibration. The modes were stepped through with increasing and decreasing frequency and the response of various forcing amplitudes were measured. The FRF response points nearest 90 degrees phase were extracted to form a NNM and the accuracy of the NNM was verified using the phase lag quadrature criterion. The linear natural frequencies and mode shapes were also obtained. This was accomplished by using the theoretical equations of motion for a circular plate with clamped boundary conditions as well as a low level modal hammer test. The results

of the hammer test were used as a benchmark to gauge a finite element models ability to predict the dynamics of the perforated plate. Once the linearity of the finite element model matched, the nonlinear dynamics of the plate were compared to the finite element model. The comparisons revealed the importance of the dynamics that could be extracted from a NNM as the NNMs generated by the finite element model and the NNMs obtained from experimental testing were very different.

A reexamination of the plate revealed that the plate was not entirely flat and an updated finite element model was created to which the results of the NNMs were improved. However, in the generated NNM it was shown that the dynamics of the plate changed from a softening nonlinearity to a hardening nonlinearity and as a result the plate was tested on a larger shaker to attempt to substantiate the model and the method of extracting NNMs at higher forcing amplitudes.

The results of the larger shaker tests were varied as the first modes dynamics started out similar to the smaller shaker tests but at higher forcing amplitudes began to show unusual behavior that could not be totally defined with just a FRF. Also, the NNMs created by the FRFs of the first mode on the larger shaker were found to be less accurate than the NNMs created by the smaller shaker. The other modes of vibration that were investigated were more linear and produced varying results; with some NNMs being as accurate as the small shaker tests and other less. In addition, it seemed that the larger shaker introduced more complications and the data collected at higher forcing amplitudes was not all that beneficial.

NNMs are a powerful tool that can be implemented by engineers in their design of structures as a linear analysis will produce a suboptimum design. They can easily be related to LNMs yet can capture nonlinear phenomena that linear techniques can overlook. The importance of a method to determine nonlinear modes is vital to the continual study of NNMs and their use in actual structural design. In most cases for the small shaker, the method presented in this thesis was able to capture the NNMs of the system with good accuracy and provide the characteristics of the nonlinear behavior of the system.

## **7. Future Work**

While the method of extracting NNMs experimentally presented in this thesis is successful there arose a number of interesting features that require further investigating. To begin with, the finite element model was never updated with the results from the large shaker tests. It would be interesting to observe if the NNMs and natural frequencies generated by the FEM would match any closer to the test specimen.

As the phase lag was not always at 90 degrees it would be useful to develop a technique to interpolate the actual 90 degree phase response based on the surrounding data points that were collected. This would theoretically produce a better estimation of the NNM.

The nonlinear behavior observed in mode one of the larger shaker tests at higher forcing amplitudes would also be an interesting feature to investigate further. As of this moment the phenomena causing the response to have an intermediate step is

unknown and may assist in explaining if multiple mode shapes are interacting at the higher forcing amplitudes. The possible turning point being observed in the first mode is also an element requiring further investigation. The stiffening of the plate was seen in the FEM but from the FRF it is unclear if that is what is actually occurring.

It is thought that the plate does not have a uniform slope from the edges of the plate to the center and therefore to further this study the actual topography of the plate should be surveyed to create a higher fidelity FEM. In conjunction with the geometry of the plate, the stresses that possibly were added to the plate during the formation of the plate and the stresses added by the orientation of the perforations should be investigated. The stresses of the plate may also be sensitive to temperature and may change orientation during operation. Characterizing these stresses and updating the FEM may be the only way to properly model the circular perforated plate and match it with the extracted NNMs.

## 8. References

---

- [1] R.M. Rosenberg, "Normal modes of nonlinear dual-mode systems," *Journal of Applied Mechanics*, vol. 27, pp. 263-268, 1960
- [2] R.M. Rosenberg, "The normal modes of nonlinear n-degree-of freedom systems," *Journal of Applied Mechanics*, vol. 29, pp. 7-14, 1962
- [3] R.M. Rosenberg, "On nonlinear vibrations of systems with many degrees of freedom," *Advances in Applied Mechanics*, vol. 9, pp. 155-242, 1966
- [4] G. Kerschen, M. Peeters, J. C. Golinval, and A.F. Vakakis, "Nonlinear normal modes, Part I: A useful framework for the structural dynamicist," *Mechanical Systems and Signal Processing*, vol. 23, pp. 170-194, 2009
- [5] Y.S. Lee, G. Kerschen, A.F. Vakakis, P.N. Panagopoulos, L.A. Bergman, D.M. McFarland, "Complicated dynamics of a linear oscillator with a light, essentially nonlinear attachment," *Physica D*, vol. 204, pp. 41-69, 2005
- [6] G. Kerschen, Y.S. Lee, A.F. Vakakis, D.M. McFarland, L.A. Bergman, "Irreversible passive energy transfer in coupled oscillators with essential nonlinearity," *SIAM Journal on Applied Mathematics*, vol. 66, pp. 648-679, 2006
- [7] M. Peeters, R. Viguie, G. Serandour, G. Kerschen, and J.C. Golinval, "Nonlinear normal modes, Part II: Toward a practical computation using numerical continuation techniques," *Mechanical Systems and Signal Processing*, vol. 23, pp. 195-216, 2009

- 
- [8] M.S. Allen, R.J. Kuether, B. Deaner, and M.W. Sracic, "A Numerical Continuation Method to Compute Nonlinear Normal Modes Using Modal Reduction", presented at the 53<sup>rd</sup> AIAA Structures, Structural Dynamics, and Materials Conference, Honolulu, Hawaii, 2012
- [9] R.J. Kuether and M.S. Allen, "A Numerical Approach to Directly Compute Nonlinear Normal Modes of Geometrically Nonlinear Finite Element Models," Mechanical Systems and Signal Processing, vol. submitted, 2013
- [10] R.J. Kuether, M.R. Brake, M.S. Allen, "Evaluating Convergence of Reduced Order Models Using Nonlinear Normal Modes," presented at the 32nd IMAC A Conference and Exposition on Structural Dynamics, Orlando, Florida, 2014
- [11] M. Peeters, G. Kerschen, and J.C. Golinval, "Dynamic testing of nonlinear vibrating structures based on nonlinear normal modes: Experimental demonstration," Mechanical Systems and Signal Processing, vol. 25, pp. 1227-1247, 2011
- [12] C. Grappasoni, J.P. Noël, G. Kerschen, "Subspace and nonlinear-normal-modes-based identification of a beam with softening-hardening behaviour," presented at the 32nd IMAC A Conference and Exposition on Structural Dynamics, Orlando, Florida, 2014
- [13] Rao, Singiresu S. *Vibration of continuous systems*. Hoboken, N.J.: John Wiley & Sons, 2007. Print.

- 
- [14] Wang, C. Y. *Structural Vibration: Exact Solutions for Strings, Membranes, Beams, and Plates*. N.p.: CRC Press, 2013. 106.EBook Library. Web. 19 Apr. 2014.
- [15] K.D. Mali, P.M. Singru, "An analytical model to determine fundamental frequency of rectangular plate having rectangular array of circular perforations," *Journal of Vibroengineering*, vol. 15, Issue 2, pp. 588-596, 2013
- [16] M.J. Jhung and J.C. Jo, "Equivalent Material Properties of Perforated Plate with Triangular or Square Penetration Pattern for Dynamic Analysis," *Nuclear Engineering and Technology*, vol. 38, October 2006
- [17] R.W. Gordon and J.J. Hollkamp, "Reduced-order Models for Acoustic Response Prediction," Air Force Research Laboratory, Dayton, OH, 2011
- [18] J.J. Hollkamp and R.W. Gordon, "Reduced-order models for nonlinear response prediction: Implicit condensation and expansion," *Journal of Sound and Vibration*, vol. 318, pp. 1139-1153, 2008
- [19] J.J. Hollkamp, R.W. Gordon, and S.M. Spottswood, "Nonlinear modal models for sonic fatigue response prediction: a comparison of methods," *Journal of Sound and Vibration*, vol. 284, pp. 1145-1163, 2005
- [20] M. Peeters, G. Kerschen, and J.C. Golinval, "Dynamic testing of nonlinear vibrating structures using nonlinear normal modes," *Journal of sound and Vibration*, vol. 30, pp. 486-509, 2011



- 
- [21] M.S. Allen, "Global and Multi-Input-Multi-Output (MIMO) Extensions of the Algorithm of Mode Isolation (AMI)," Ph.D., George W. Woodruff School of Mechanical Engineering, Georgia Institute of Technology, Atlanta, Georgia, 2005
- [22] M. Amabili, R. Pierandrei, G. Frosali, "Analysis of Vibrating Circular Plates Having Non-Uniform Constraints Using The Modal Properties of Free-Edge Plates: Application to Bolted Plates," *Journal of Sound and Vibration*, pp 23-28; 1997

---

## Appendix A

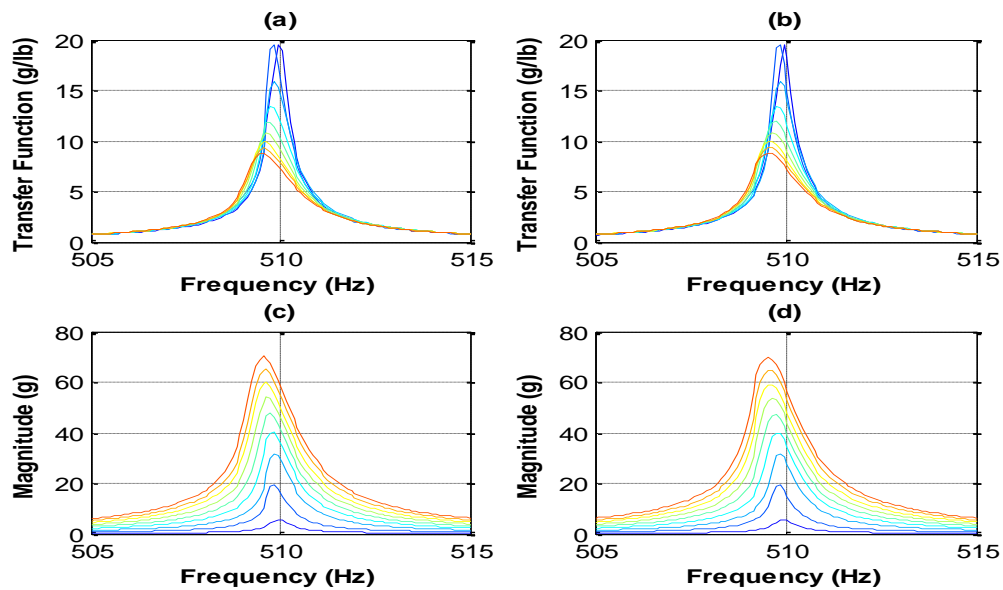


**Figure 37: Transfer function of fifth mode stepping (a) up (b) down in frequency.**

**FRFs of fifth mode stepping (c) up (d) down in frequency**

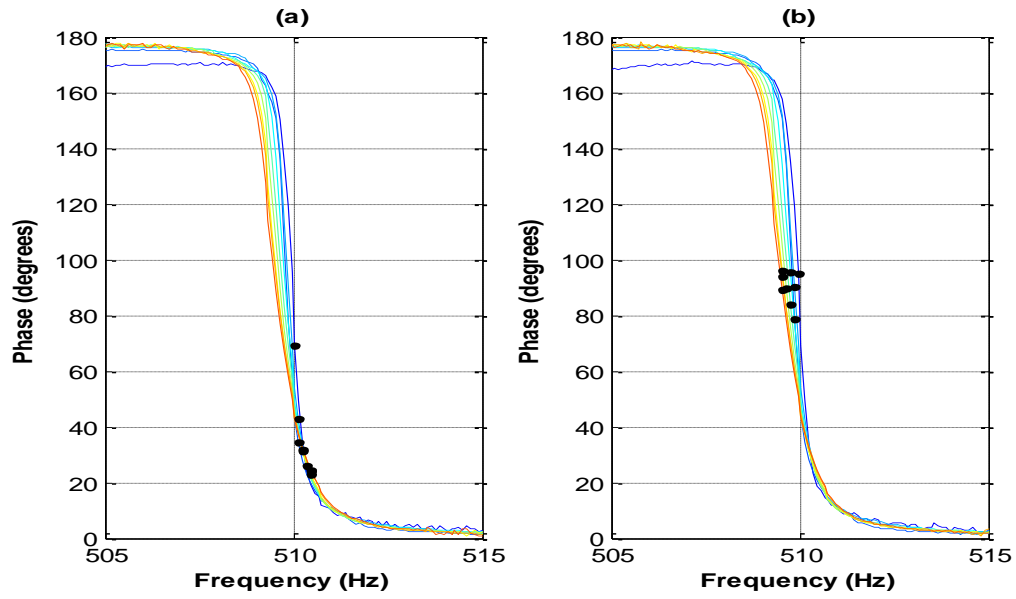


**Figure 38: Phase lag of the fifth mode (a) stepping up. (b) stepping down in frequency. Markers indicate points of the fifth mode from which the NNM was extracted**